Kinetics Study of MoS_2 and $MoSe_2$ Electrocatalysts to Determine the Mechanistic Steps for Hydrogen Evolution Reaction (HER) via Simulation

Zerzes Verscera
anak Make

Bachelor of Engineering
Chemical Engineering and Energy Sustainability

UNIVERSITI MALAYSIA SARAWAK

- Grade: _____

Please tick (√)	
Final Year Project Report	√
Masters	
PhD	

DECLARATION OF ORIGINAL WORK

This declaration is made on the 24th day of JUNE 2023.

- **Student's Declaration**:

I, ZERZES VERSCERA ANAK MAKE (72739), DEPARTMENT OF CHEMICAL ENGINEERING AND ENERGY SUSTAINABILITY, FACULTY OF ENGINEERING hereby declare that the work entitled, KINETICS STUDY OF MoS_2 AND $MoSe_2$ ELECTROCATALYSTS TO DETERMINE THE MECHANISTIC STEPS FOR HYDROGEN EVOLUTION REACTION (HER) VIA SIMULATION is my original work. I have not copied from any other students' work or from any other sources except where due to reference or acknowledgement is made explicitly in the text, nor has any part been written for me by another person.

30 JUNE 2023	ZERZES VERSCERA ANAK MAKE (72739)
Date submitted	Name of the student (Matric No.)

Supervisor's Declaration:

I, HARUNAL REJAN BIN RAMJI hereby certifies that the work entitled, KINETICS STUDY OF MoS_2 AND $MoSe_2$ ELECTROCATALYSTS TO DETERMINE THE MECHANISTIC STEPS FOR HYDROGEN EVOLUTION REACTION (HER) VIA SIMULATION was prepared by the above named student, and was submitted to the "FACULTY" as a fulfilment for the conferment of BACHELOR OF ENGINEERING WITH HONOURS (CHEMICAL ENGINEERING), and the aforementioned work, to the best of my knowledge, is the said student's work

Received for examination by: HARUNAL REJAN BIN RAMJI

(Name of the supervisor)

Date: 30 JUNE 2023

I declare this Report is classified as (Please tick (√)):

☐ **CONFIDENTAL** (Contains confidential information under the Official Secret Act 1972)*

☐ **RESTRICTED** (Contains restricted information as specified by the organization where was done)*

☑ **OPEN ACCESS**

Validation of Report

I therefore duly affirmed with free consent and willingness declared that this said Report shall be placed officially in Department of Chemical Engineering and Energy Sustainability with the abide interest and rights as follows:

- This Report is the sole legal property of Department of Chemical Engineering and Energy Sustainability, Universiti Malaysia Sarawak (UNIMAS).
- The Department of Chemical Engineering and Energy Sustainability has the lawful right to make copies for the purpose of academic and research only and not for other purpose.
- The Department of Chemical Engineering and Energy Sustainability has the lawful right to digitise the content to for the Local Content Database.
- The Department of Chemical Engineering and Energy Sustainability has the lawful right to make copies of the Report for academic exchange between Higher Learning Institute.
- No dispute or any claim shall arise from the student itself neither third party on this Report once it becomes sole property of Department of Chemical Engineering and Energy Sustainability, Universiti Malaysia Sarawak (UNIMAS).
- This Report or any material, data and information related to it shall not be distributed, published or disclosed to any party by the student except with Department of Chemical Engineering and Energy Sustainability, Universiti Malaysia Sarawak (UNIMAS) permission.

Student's signature:_____ Supervisor's signature: _____

(30 JUNE 2023) (30 JUNE 2023)

Current Address:

DEPARTMENT OF CHEMICAL ENGINEERING & ENERGY SUSTAINABILITY, FACULTY OF ENGINEERING, UNIVERSITI MALAYSIA SARAWAK, 94300 KOTA SAMARAHAN, SARAWAK

Notes: ***** If the Report is **CONFIDENTIAL** or **RESTRICTED**, please attach together as annexure a letter from the organisation with the period and reasons of confidentiality and restriction.

- APPROVAL SHEET

-

This final year project report which entitled **"Kinetics Study of MoS_2 and $MoSe_2$ Electrocatalysts to Determine the Mechanistic Steps for Hydrogen Evolution Reaction (HER) via Simulation"** was prepared by student's name as partial fulfilment for the Degree of Bachelor of Engineering with Honours (Chemical Engineering) is hereby read and approved by:

30 JUNE 2023

Date

Harunal Rejan bin Ramji

(Final Year Project Supervisor)

KINETICS STUDY OF MOS_2 AND $MOSE_2$ ELECTROCATALYSTS TO DETERMINE THE MECHANISTIC STEPS FOR HYDROGEN EVOLUTION REACTION (HER) VIA SIMULATION

ZERZES VERSCERA ANAK MAKE

A dissertation submitted in partial fulfilment
of the requirement for the degree of
Bachelor of Engineering with Honours
Chemical Engineering

Faculty of Engineering

Universiti Malaysia Sarawak

2023

Dedicated to my beloved family, supervisor, lecturers, and friends who gave continuous motivations and encouragements upon completion of this project.

ACKNOWLEDGEMENT

The students wish to express his utmost gratitude and appreciation to Dr. Harunal Rejan bin Ramji as the student's supervisor for this project. The student also wishes to express their gratitude to Universiti Malaysia Sarawak (UNIMAS), the Faculty of Engineering and the lecturers who have provided guidance for success of this project.

ABSTRACT

The higher energy yield of hydrogen makes it an appealing substitute for fossil fuels, and its combustion doesn't produce dangerous pollutants like carbon monoxide and nitrogen oxides. But traditional production techniques like steam methane reformation use fossil fuels, which are not a renewable resource in and of themselves and emit carbon dioxide. As an alternative, hydrogen could be produced through the electrolysis of water, which involves splitting the water molecules into oxygen and hydrogen gas using an electrical current. The performance of the reaction is influenced by the electrode material, or electrocatalyst, and the performance of the electrocatalyst is assessed using the overpotential, exchange current density, and Tafel slope. The best electrocatalysts, like platinum, have the highest exchange current densities, the lowest overpotentials, and Tafel slopes. The scarcity and costs of platinum resulted in the development of alternative materials. In this project, COMSOL Multiphysics software is used to determine the electrocatalytic properties of molybdenum sulfide, MoS_2, and molybdenum selenide, $MoSe_2$, and compare it with platinum. From the simulation, it is found that the Tafel slope, the overpotential and the exchange current density for MoS_2 are 118 mV per decade, 1.4 mV, and 3.47 x 10^{-3} mA/cm^2, respectively. While for $MoSe_2$, the values for these parameters are 111 mV per decade, 0.74 mV, and 3.31 x 10^{-3} mA/cm^2, respectively.

Keywords: Hydrogen evolution reaction, electrocatalyst, overpotentials, exchange current density, Tafel slope

ABSTRAK

Hidrogen adalah alternatif yang sesuai untuk bahan bakar fosil kerana mempunyai hasil tenaga yang lebih tinggi dan pembakarannya tidak melepaskan bahan pencemar berbahaya seperti karbon monoksida dan nitrogen oksida. Walau bagaimanapun, kaedah pengeluaran konvensional seperti reformasi metana wap menggunakan bahan bakar fosil, iaitu sumber yang tidak boleh diperbaharui, serta melepaskan karbon dioksida. Sebagai alternatif, elektrolisis air digunakan untuk menghasilkan hidrogen dengan memisahkan molekul air menjadi gas oksigen dan gas hidrogen melalui arus elektrik. Bahan elektrod, atau elektrokatalis, mempengaruhi prestasi tindak balas, dan prestasi elektrokatalis diukur berdasarkan potensi lebihan, ketumpatan arus pertukaran dan cerun Tafel. Elektrokatalis terbaik mempunyai potensi lebihan dan cerun Tafel yang rendah, dan ketumpatan arus pertukaran yang tinggi, seperti platinum. Walau bagaimanapun, sumber platinum yang terhad beserta kos yang tinggi membawa kepada pengembangan bahan alternatif sebagai pengganti platinum. Dalam projek ini, perisian COMSOL Multiphysics digunakan untuk menentukan sifat elektrokatalitik molibdenum sulfida, MoS_2, dan molibdenum selenida, $MoSe_2$, dan membandingkannya dengan platinum. Dari simulasi ini, ia didapati bahawa cerun Tafel, potensi lebihan dan kepadatan arus pertukaran untuk MoS_2 masing-masing adalah 118 mV per dekad, 1.4 mV, dan 3.47 x 10-3 mA / cm^2. Manakala, untuk $MoSe_2$, nilai untuk parameter-parameter ini masing-masing adalah 111 mV per dekad, 0,74 mV, dan 3,31 x 10-3 mA/cm^2.

Kata Kunci: Reaksi evolusi hidrogen, elektrokatalis, potensi lebihan, ketumpatan arus pertukaran, cerun Tafel

TABLE OF CONTENTS

LIST OF TABLES

LIST OF FIGURES

LIST OF ABBREVIATIONS

OPEC	Organization of the Petroleum Exporting Countries
SMR	Steam Methane Reformation
LCA	Life Cycle Analysis
LHV	Lower Heating Value
RES	Renewable Energy Resources
HER	Hydrogen Evolution Reaction
TOF	Turnover Frequency
DFT	Density Functional Theory
NW	Nanowire
GCE	Glassy Carbon Electrode
GUI	Graphical User Interface
VHT	Volmer-Heyrovsky-Tafel

Chapter 1 Introduction

1.1) Background

Nowadays, natural gases and fossil fuels have become staples in fulfilling energy requirements. Nonetheless, the utilization of fossil fuels emits greenhouse gases, nitrogen dioxides, and sulphur dioxides. These pollutants are known to cause global warming, acid rain, and air pollution. Furthermore, the global distribution of fossil fuels is not conducted adequately, and there are also rising concerns regarding the security of their supply as these resources are majorly obtained from the OPEC, the Organization of the Petroleum Exporting Countries (Pareek et al, 2020). Other concerns pointed out by Pareek et al are global competition and increases in prices due to its finite availability. Sazali (2020) states that the utilization of fossil fuels requires a longer time to recharge. These issues indicate the unsustainability of fossil fuels as the main energy resource. As an alternative, hydrogen is deemed as the most suitable candidate as it is renewable and more environmentally friendly. The combustion produced water vapour instead of greenhouse gasesand the energy yield was found to be almost 3 times higher than hydrocarbon fuels, about 122 kJ/g (Sazali, 2020). The main resources for hydrogen are water, oil, and gas. With water being the most abundant resource, hydrogen could be produced locally, and non-oil-producing countries could become more independent in generating their energy and reduce their reliance on foreign energy suppliers (Revankar, 2019).

The most common method of producing hydrogen, about 80% to 85% of the globally produced hydrogen, is through steam methane reforming (SMR) due to its low cost (Sazali, 2020). According to Ajanovic & Haas (2018), approximately 55% of the hydrogen produced globallyis utilized in ammonia synthesis, 25% for refineries, 10% for methanol synthesis, and the remainder is used for other applications. During SMR, steam is maintained at a temperature and pressure between 700 - 1000℃ and 3 – 25 bar. The reaction of steam with methane or other hydrocarbons produces hydrogen, carbon monoxide, and carbon dioxide. Carbon monoxide and steam undergo another reaction over the catalyst to further increase the hydrogen yield. Shown below are the reactions involved in SMR:

$$CH_4 + H_2O \rightarrow CO + 3H_2 \qquad \text{(Eq 1.1)}$$

$$CO + H_2O \rightarrow CO_2 + H_2 \qquad \text{(Eq 1.2)}$$

However, SMR is considered unsustainable because it requires fossil fuel, which itself is a finite resource. Furthermore, SMR is responsible for high CO_2 emissions and high energy consumption. Based on a direct facility-level emissions analysis by Cho, Strezov & Evans (2022) conducted on 33 facilities in the USA, the impact values of SMR were 9.35 kg CO_2/kg H_2. As for the life cycle analysis (LCA), only 0.66 MJ of hydrogen is generated for every 1 MJ of fossil fuel burned, based on the lower heating value (LHV) basis (Spath & Mann, 2000). Based on the study by Spath & Mann, **Table 1.1** shows the hydrogen plant energy balance while **Figure 1.1** shows the CO_2 equivalent emissions of various operations.

Table 1.1 Energy Balance of Hydrogen Plant (Spath & Mann, 2000)

	Base case result
Life cycle efficiency	-39.6%
External energy efficiency	60.4%
Net energy ratio	0.66
External energy ratio	5.1

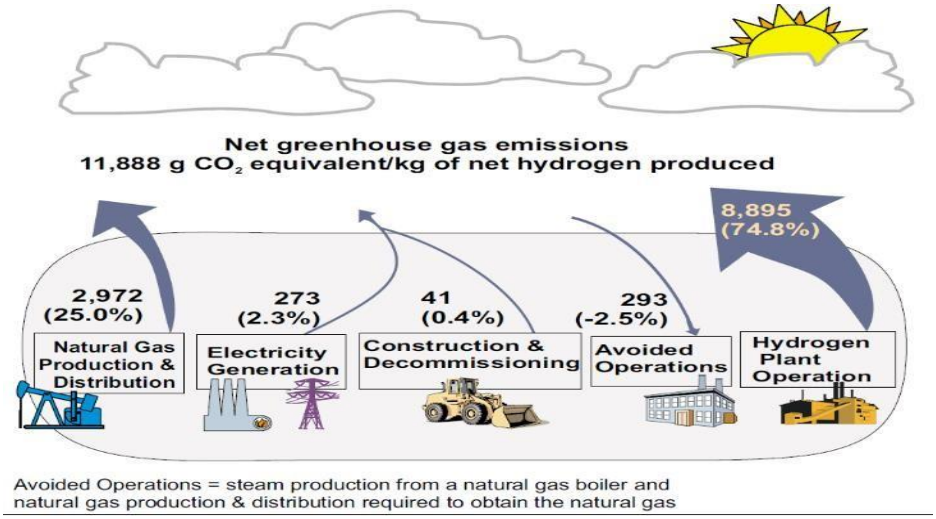

Figure 1.1 CO_2 Equivalent Emissions of Various Operations (Spath & Mann, 2000)

For a more feasible alternative, water splitting through electric current should be considered. In this process, electric current is applied on water to initiate its separation into gaseous hydrogen and oxygen. According to Pareek et al (2020), the synthesis of hydrogen via electrolysis could potentially have zero emissions of greenhouse gases, depending on the source used to provide electricity. The rapid growth renewable energy resources (RES) as a means to produce electricity resulted in the imbalance of electricity supply and demand by reducing the cost of the energy generated, thus providing the opportunity for the utilization of RES as an electricity source for hydrogen production (Ajanovic & Haas, 2018). Below are the reactions involved inwater electrolysis (Pareek et al, 2020):

$$Electrolyte: 4H_2O \rightarrow 4H^+ + 4OH^- \quad \text{(Eq. 1.3)}$$

$$Cathode: 4H^+ + 4e^- \rightarrow 2H_2 \quad \text{(Eq. 1.4)}$$

$$Anode: 4OH^- \rightarrow O_2 + 2H_2O + 4e^- \quad \text{(Eq. 1.5)}$$

$$Overall: 2H_2O \rightarrow O_2 + 2H_2 \quad \text{(Eq. 1.6)}$$

The cathodic reaction is the hydrogen evolution reaction (HER), which will be the focus of this research. During HER, the hydrogen is adsorbed at the electrode surface. Also, the adsorption energy is dependent on the materials of the electrode.

The parameters that determined the efficiency of an electrocatalyst in HER are the Tafel slope, overpotentials, and current densities. The exchange current density, j_0, is the measurement of electrical current per unit area (Vesborg, Seger, & Chorkendorff, 2015). Overpotential, η, is the equilibrium potential minus the applied potential, or the activation energy barrier, while the Tafel slope, b, is the necessary additional overpotential to increase the current density by tenfold (Zeng & Li, 2015). Each of these parameters is represented by the equations below (Zeng & Li, 2015):

$$j_0 = \frac{j}{-e^{-\frac{\alpha nF\eta}{RT}} + e^{(1-\alpha)nF\eta/RT}} \quad \text{(Eq. 1.7)}$$

$$\eta = \left(\frac{RT}{nF j_0}\right) j \quad \text{(Eq. 1.8a) or}$$

$$\eta = a + b\,logj = \frac{-2.3RT}{\propto nF}\log(j_0) + \frac{2.3RT}{\propto nF}\log(j) \quad \text{(Eq. 18b)}$$

With j representing the current density, α representing the coefficient for charge transfer, F representing Faraday's constant, n (usually equal to 1) representing the electrons transferred, R being the ideal gas constant, and T being the temperature.

The best electrocatalyst is the one with a smaller overpotential, higher exchange current density, and lower Tafel slope and Pt-based catalyst has an overpotential of almost zero and a Tafel slope of around 30 mV/dec (Efthekari, 2017), making it the ideal electrocatalyst for HER. However, finding and developing cheaper alternatives has become a major interest as Pt is a very expensive and scarce resource. According to Vesborg, & Jaramillo (2012), the annual global production of platinum is 180 tons/yr.

For this research, the focus will be on the comparison between two Mo-based catalysts (-S_2 and -Se_2) and the Pt. A simulation will be conducted to determine the electrocatalytic properties of these materials and compared them with the finding in a previous study, particularly from Kong et al (2013). The simulation is expected to display a Tafel slope of between 105 – 120 mV/dec and the exchange current density of 2.2 x 10^{-2} mA/cm^2 is obtained for MoS_2 and 2.0 x 10^{-2} mA/cm^2 for $MoSe_2$.

1.2) Problem Statement

The most efficient electrocatalyst for HER is the Pt-based electrocatalyst. Nonetheless, the scarcity of the resources and its high costs the utilization of Pt-based electrocatalysts for HER in a long-term and/or large-scale operation considered economically infeasible. Therefore, a cheaper and more readily available substitute with a comparable performance has become the priority in developing electrocatalysts for HER.

As most transition metal compounds possess low electrical conductivities, enhancement of the electrical conductivities becomes the focus in developing these materials as a substitute form Pt in HER (Eftekhari, 2017). Also, according to Eftekhari, the main problems faced in developing alternative electrocatalysts are increasing the active site while simultaneously enhancing the conductivity and reducing the required overpotential.

The development of a cheaper and comparably efficient electrocatalyst for HER is significant in the energy sector, especially in the generation of energy. As described by Yue et al (2021), there are various resources of hydrogen and with water being the most widely available, non-oil-producing countries could harness it as their energy resources through

electrocatalysis. For this research, the more efficient substitute for Pt for electrocatalyst will be determined through a simulation based on its overpotential, current density, and Tafel slope.

1.3) Hypothesis

Our research suggests that surface diffusion between the doped materials and based materials causes the improved HER performances.

1.4) Objectives

For this research, there are two objectives to be accomplished. They are:

1) To determine the electrocatalytic properties of MoS_2 and $MoSe_2$ electrocatalysts through simulation, and
2) To differentiate the performance of the electrocatalysts with Pt

1.5) Research Gap

The research gap for this study is the utilization of simulation software to determine the accuracy of the results obtained by Kong et al in 2013. The study was conducted in a laboratory setting and the calculation for the overpotentials, exchange current densities, and Tafel slope was conducted based on the experimental results. Therefore, the simulation aimed to verify the results by incorporating the Volmer-Heyrovsky-Tafel (VHT) mechanistic steps theoretical approach and explain the improved HER performances of doped materials.

1.6) Scope of Study

The scope of this study incorporates simulation of the effect of modifications of Mo-based electrocatalysts on HER. The simulation will be conducted with the COMSOL Multiphysics software to examine the effect of surface diffusion on doped materials.

1.7) Chapter Summary

Regarding the environmental impact, the production of hydrogen through electrolysis is a better alternative compared to steam methane reformation due to the latter emits a high amount of greenhouse gases and has a high fuel consumption. Pt is regarded as the best electrocatalyst for electrolysis. The high cost and limited resources for Pt push research and development of cheaper and equivalently efficient electrocatalysts for long-term utilization. In

this study, the electrocatalytic properties of MoS_2 and $MoSe_2$ will be tested using the COMSOL Multiphysics software.

Chapter 2 Literature Review

2.1) Hydrogen Evolution Reaction (HER)

HER involves the Volmer reaction, superseded by Heyrovsky reaction or Tafel reaction, resulting in hydrogen formation (Eftekhari, 2017). During Volmer, adsorption of hydrogen occurs at the electrocatalyst surface. In Tafel and Heyrovsky reaction, the hydrogen is desorbed from the electrocatalyst surface, in an electrochemical and chemical manner respectively.

HER may be conducted in either acidic or basic solutions (Lasia, 2019). In an acidic solution, protons are reduced to gaseous dihydrogen gas at the cathode (Dubouis & Grimaud, 2019). For the Volmer step, the reduction of the proton takes place at the active site on the catalyst surface, followed by either the Heyrovsky step, where another proton or electron is being transferred, or the Tafel step, the reunification of the two adsorbed proton. Below are the equations for all three reactions (Lasia, 2019):

$$Volmer:\ H^+ + M + e^- \leftrightarrow MH_{ads} \quad \text{(Eq. 2.1)}$$

$$Tafel:\ 2MH \leftrightarrow 2M + H_2 \quad \text{(Eq. 2.2)}$$

$$Heyrovsky: MH + H^+ + e^- \leftrightarrow M + H_2 \quad \text{(Eq. 2.3)}$$

As for alkaline media, the proton concentration is excessively decreased (Dubouis & Grimaud, 2019). Both in acidic and alkaline media, hydrogen production involves Volmer and Tafel or Heyrovsky steps. However, the Volmer step in an alkaline media involves an additional component where the water O-H bond is dissociated. Below are the equations for all three reactions (Lasia, 2019):

$$Volmer:\ H_2O + M + e^- \leftrightarrow MH_{ads} + OH^- \quad \text{(Eq. 2.4)}$$

$$Tafel:\ 2MH \leftrightarrow 2M + H_2 \quad \text{(Eq. 2.5)}$$

$$Heyrovsky: MH + H_2O + e^- \leftrightarrow M + OH^- + H_2 \quad \text{(Eq. 2.6)}$$

The HER performance is measured based on the electrocatalytic properties of the electrocatalysts, which are comprised of the, the Tafel slope, the exchange current density, and the overpotential. Lower overpotentials indicate higher efficiencies, and as a figure of merit, a potential to reaches a current of 10 mA/cm^2 is generally used as a basis for measuring electrocatalytic activity.

Another consideration is the operating costs. Commercially, the current density for a general operation is within the range of 1 – 10 A/cm^2, which results in a high operating voltage requirement, and the additional cost due to the high voltage could be balanced out by savings on capital costs, as a smaller electrolyzer size is required for an operation with higher current density (Vesborg, Seger, & Chorkendorff, 2015). A similar study also reveals that higher current density increases the ohmic losses due to the inefficiency in transferring ions in the electrolyte. To mitigate this problem, the authors recommended the utilization of a highly conductive electrolyte such as a highly acidic or basic media, although acidic media is preferable as it is more conductive.

It is also important to consider the catalyst cost in choosing the electrocatalyst. The costs can be categorized as soft costs and hard costs. The soft costs are the cost of catalysts' synthetic preparation, while the hard costs are the market price for the constituent elements. The soft costs can be reduced by changing production methods, while for the hard costs, the utilization of naturally abundant materials is usually cheaper.

2.2) Electrocatalysts in HER

In HER, an electrocatalyst could reduce the overpotentials and stimulate the reaction rate and its efficiency. Electrocatalyst itself can be either homogeneous or heterogeneous. In this section, various derivatives of Mo-based electrocatalysts will be discussed along with another alternative metal such as a W-based electrocatalyst.

2.2.1) Mo-based Electrocatalysts in HER

Mo itself is cheaper and more commonly found on Earth. Mo-based electrocatalyst itself displays a Pt-like behaviour, making it a comparative candidate for an alternative to Pt (Bae et al, 2018). The following are the Mo derivatives which display excellent performance in HER.

2.2.1.1) Mo-based Sulphides

For Mo-based sulphides, the most used is molybdenum disulphides, MoS_2. The active sites for HER are the edge site of the material (Hua et al, 2020). However, MoS_2 basal planes are almost inactive, and more thermodynamically stable in comparison with the active edge planes (Zhuang et al, 2019, Hua et al, 2020). MoS_2 electrocatalytic performance can be enhanced by multiplying the quantity of available active sites and improving the innate catalytic activity and the catalytic conductivity and diffusion properties (Zhuang et al, 2019).

To multiply the available active sites, Kong et al (2013) develop a MoS_2 film with vertically aligned nanosheets which provides a great supply of active exposed edge sites. Illustrated in **Figure 2.1,** the material displays a Tafel slope of 120 mV/dec. The material also possesses an exchange current density of 2.2 x 10^{-3} mA/cm^2.

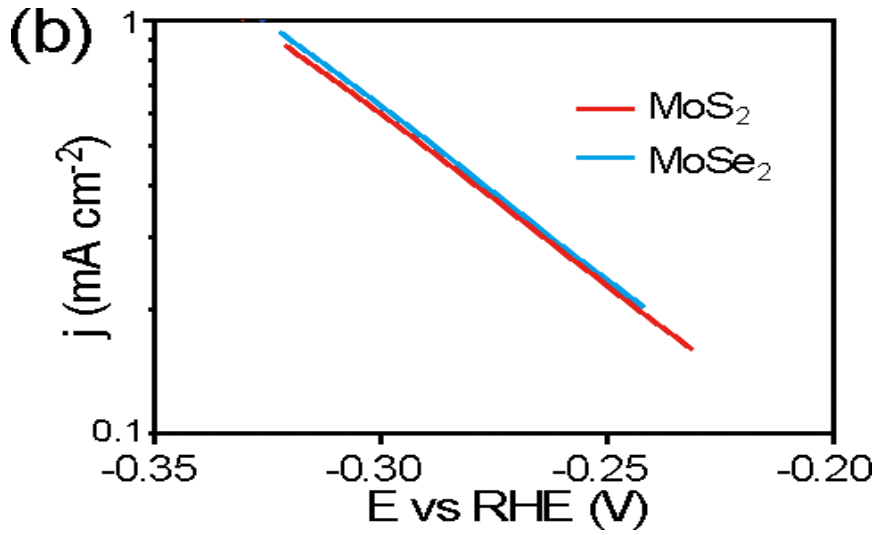

Figure 2.1 MoS_2 Tafel slope (Kong et al, 2013)

Metal doping could stimulate the HER activity of the basal plane and allow the catalysis by the adjacent S-edge site (Zhuang et al, 2019). In an alkaline solution, doping of nickel atoms could enhance the kinetics of water dissociation of MoS_2 (Zhang et al, 2016). The overpotential obtained is 98 mV at 10 mA/cm^2. Furthermore, anion doping such as oxygen atoms doped with MoS_2 phase disorder could optimize the HER activity (Xie et al, 2013). The author discovered that the phase disorder catalytically activates the unsaturated S atoms, and the O atoms promote high electron mobility of the sulphides basal plane, along with enhancement of intrinsic conductivity. The overpotential of this material is 120 mV and the Tafel slope is 55 mV/dec. **Figure 2.2** displays the Tafel slope of Xie et al findings.

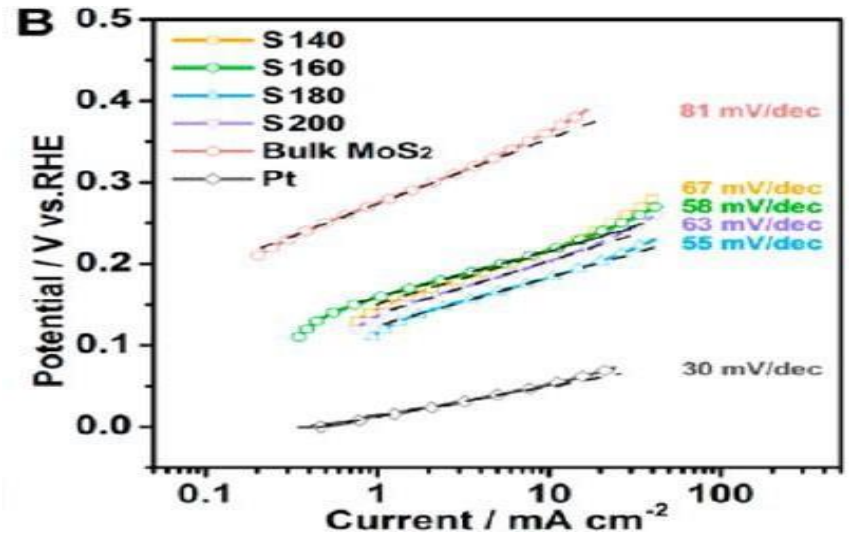

Figure 2.2 Tafel plots of oxygen-doped MoS_2 ultrathin nanosheets (Xie et al, 2013)

Due to the MoS_2 natural semiconductor structure, the 2H phase of MoS_2 possesses a substandard conductivity, which restricts its catalytic activity (Hua et al, 2020). To improve the conductivity, Sun et al (2014) doped vanadium (V) atoms into the MoS_2 interlayer. The doping is found to not only enhance the conductivity but also its overpotential and Tafel slope, which being 130 mV and 69 mV/dec, respectively. The Tafel plot is presented as **Figure 2.3.**

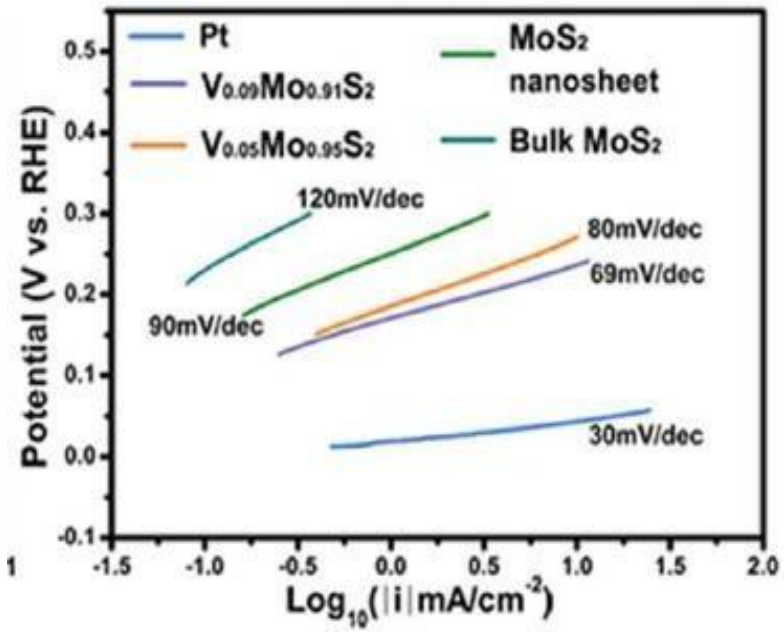

Figure 2.3 Tafel plots of V-doped MoS_2 interlayer in comparison with Pt, MoS_2 nanosheet, and Bulk MoS_2 (Hua et al, 2020)

2.2.1.2) Mo-based Selenides

As both Se and S are elements of the same group, $MoSe_2$ and MoS_2 shares identical properties and could have a comparable catalytic performance toward HER (Hua et al, 2020). However, Zhang et al (2019) reveal that two factors inhibit the $MoSe_2$ from reaching its full potential on HER. These factors are the inactivity of the bulk $MoSe_2$, due to an insufficiency of exposed edge sites, and very slow kinetics at higher current density due to the proportionately inadequate conductivity and the 2H phase strong contact resistances.

$MoSe_2$ nanosheets with additional Se vacancy possess an overpotential of approximately 170 mV along with the Tafel slope of 98 mV/dec (Zhou et al, 2014). Alternatively, doping $MoSe_2$ nanosheets with sulphur could not only improve its conductivity but also provides an electrocatalyst possessing 156 mV of overpotential at 30 mA/cm^2 along with a Tafel slope of 58 mV/dec (Xu et al, 2014). The Tafel plots for both findings are illustrated as **Figure 2.4** & **2.5**

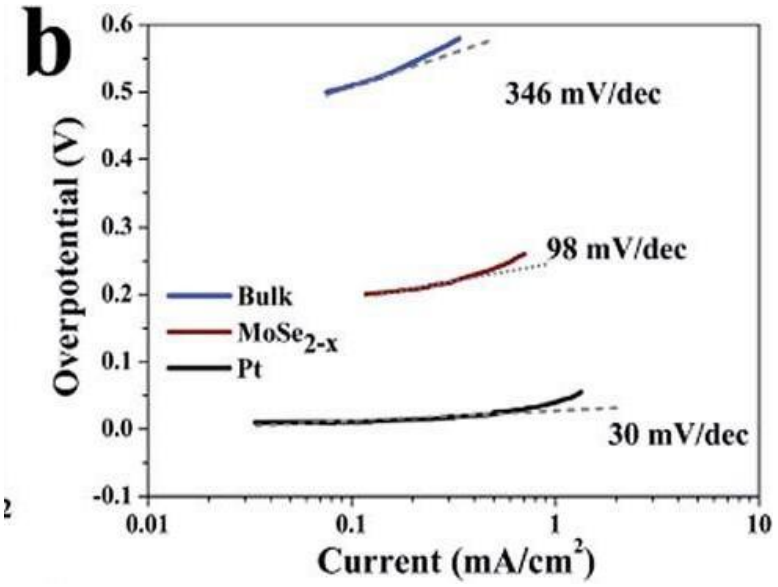

Figure 2.4 Tafel plots of bulk $MoSe_2$, Pt, and $MoSe_2$ nanosheets with additional Se vacancy (Zhou et al, 2014)

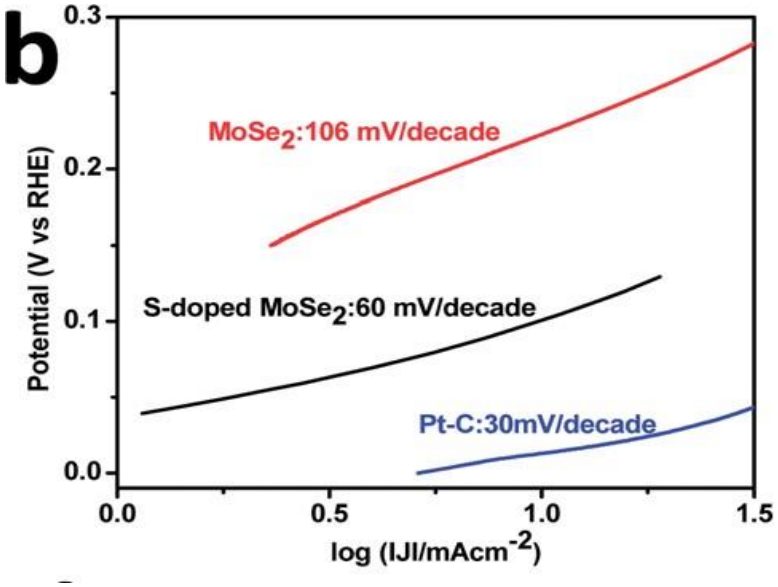

Figure 2.5 Tafel plots of $MoSe_2$, S-doped $MoSe_2$ and Pt-C (Xu et al, 2014)

Additionally, the enhancement of electrical conductivity is also achievable with the insertion of the metallic 1T phase into the 2H phase via N-doping (Zhang et al, 2019). The doping resulted in the development of N-doped $MoSe_2$ nanoflakes of 98 mV for overpotential, a Tafel slope of 49 mV/dec, enhanced durability, and abundant active sites.

Another study that involved N-doping by Deng et al (2018) describes the

development of an N-doped $MoSe_2$/TiC-C shell/core array, with the TiC-C nanorod arrays serving as the foundation for the $MoSe_2$ nanosheets. The material displays an overpotential of 137 mV, when the current density reaches 100 mA/cm^2. The Tafel slope obtained is 32 mV/dec, as shown by **Figure 2.6**

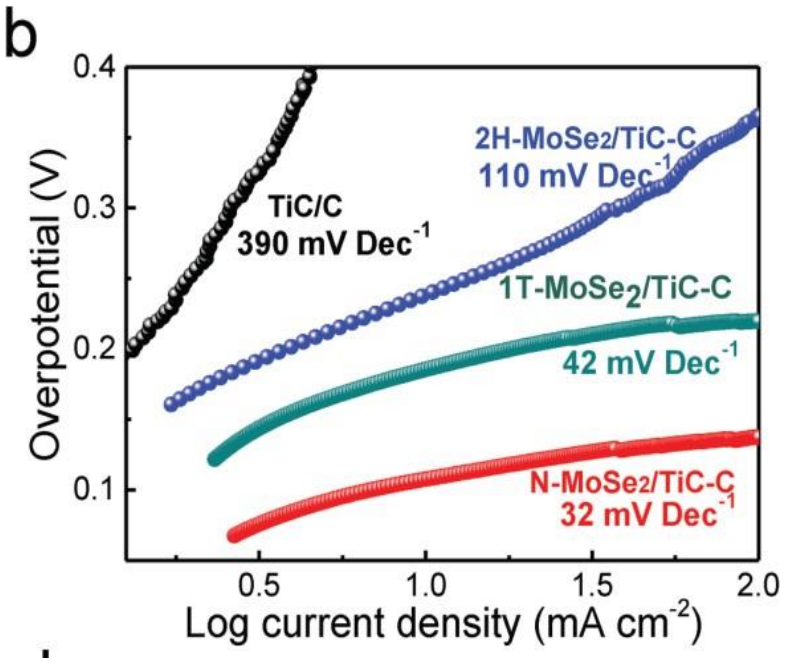

Figure 2.6 Tafel plots for the TiC-C, 1T-$MoSe_2$/TiC-C, 2H-$MoSe_2$/TiC-C, and N-$MoSe_2$/TiC-C (Deng et al, 2018)

A study by Nguyen et al (2018) describes the development of amorphous molybdenum selenide nanopowder, which was developed from reflux of $Mo(Co)_6$ and Se precursors in dichlorobenzene. In the study, the material displays an enhancement in its HER ability. In a neutral pH, only 270 mV of overpotential at 10 mA/cm^2 of current density and the displayed Tafel slope is 60 mV/dec.

2.2.1.3) Mo-based Carbides

According to Miao et al (2017), DFT (density functional theory) calculations of molybdenum carbides (Mo_xC) displays that the broadening of the d-band structures via hybridization of molybdenum and molybdenum s- and p-orbitals of carbons causes the carbides to achieve an identical d-band structure to those of Pt, indicating electrocatalytic

properties of thecarbides are akin to Pt.

Liao et al (2013) describes the development of nanoporous carbide nanowires (np-Mo_2C NWs) through the pyrolysis of MoO_x/amine hybrid precursor alongside sub-nanosized periodic structure subjected to an inert atmosphere. The HER activity is analyzed by setting the material down on a glassy carbon electrode (GCE) with a catalyst loading of 0.21 mg/cm^2, forming an np-MO_2C NW-modified GCE. The study reveals that the material displays an overpotential of 200 mV at a current density of 60 mA/cm^2. Combined with commercial Vulcan carbon at 1:1 w/w, the np-Mo_2C NW-modified GCE displays an enhancement in its electrocatalytic properties. This includes a current density of 80 mA/cm^2 at an overpotential of 200 mV and a Tafel slope of 54 mV/dec, as shown in **Figure 2.7**.

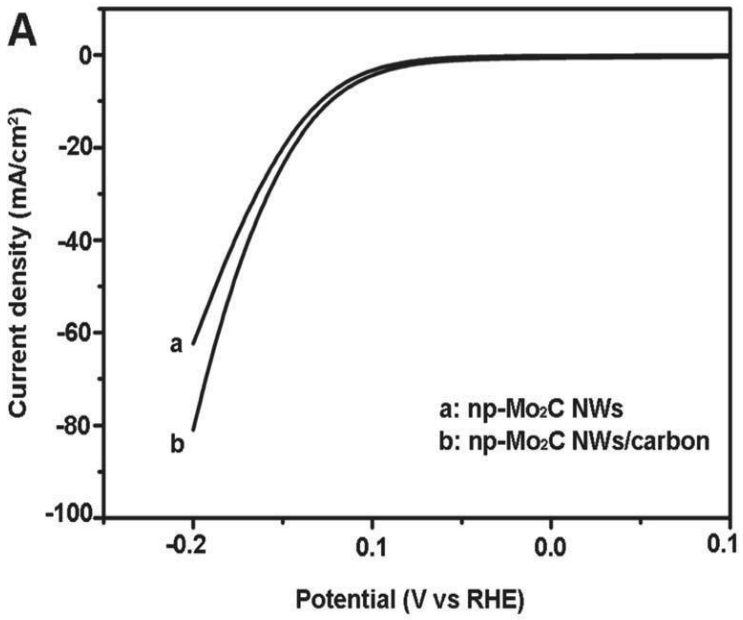

Figure 2.7 Tafel plots of np-Mo_2C NWs and np-Mo_2C NWs/carbon (Liao et al, 2013).

Wan, Regmi, and Leonard (2014) compare the four phases of Mo-C in terms of its electrocatalytic properties in HER. The phases are α-MoC_{1-x}, β-Mo_2C, η-MoC and γ-MoC. Among the four phases, γ-MoC is found to be the most stable. The exchange current density obtained is 3.2 μA/cm^2 and the Tafel slope being 121.6 mV/dec, as shown on **Figure 2.8**, with the overpotentials ranging from 270 mV – 310 mV.

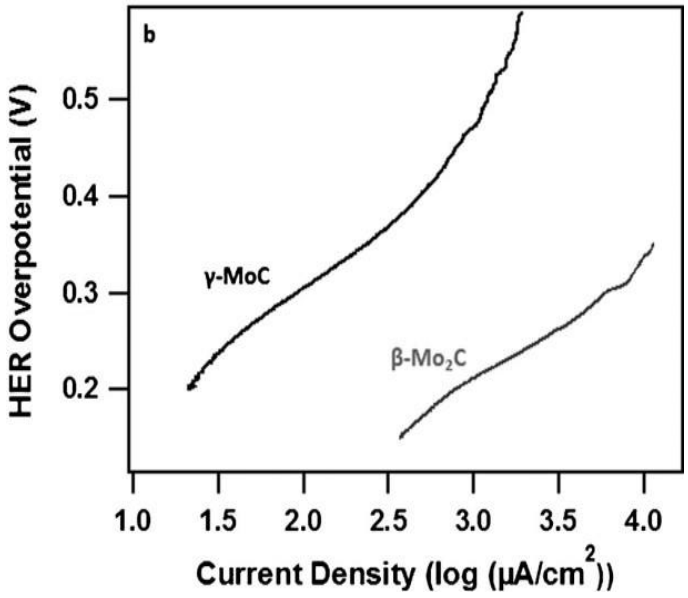

Figure 2.8 Tafel plots of γ-MoC and β-Mo_2C (Wan, Regmi & Leonard, 2014)

The doping of Mo_2C with iron by Wan and Leonard (2015) through an amine-metal oxide composite method also displays an enhancement in electrocatalytic properties for molybdenum carbides. Utilizing β-Mo_2C doped with iron (Fe-doped β-Mo_2C) illustrates a small current of -0.15 mA - -0.25 mA at a low potential of -140 mV. **Figure 2.9** illustrates the Tafel plot of iron-doped Mo_2C.

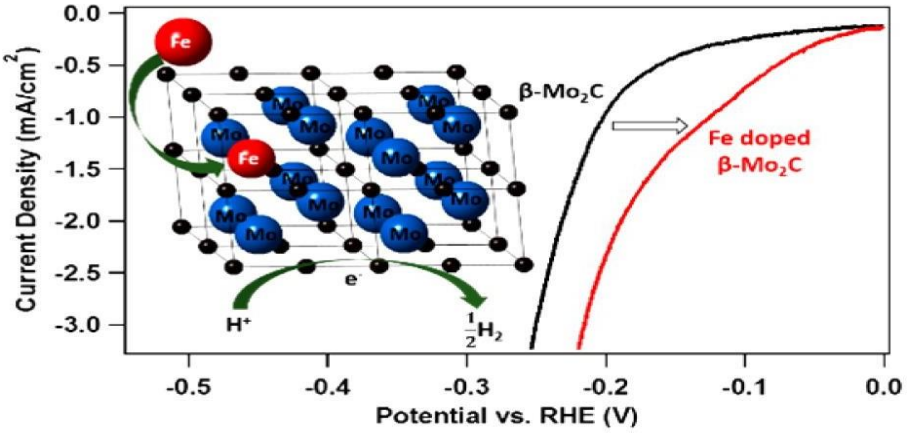

Figure 2.9 Tafel plot of Fe-doped Mo_2C and β-Mo_2C (Wan & Leonard, 2015)

2.2.2) W-based Electrocatalysts in HER

Another alternative for Pt is W-based electrocatalyst. This section will discuss the carbides, oxides, and sulfides of tungsten.

2.2.2.1) W-based Carbides

In a study by Emin et al in 2018, the authors prepared colloidal tungsten nanoparticles (W NPs) which were then spin-coated on graphite electrodes. The resulting material then undergoes heat treatment at an elevated temperature of 900 ℃ and above, producing tungsten metal and its carbide (W_2C/WC) thin films. The HER performance test is carried out in an acidic condition of 0.5 M H_2SO_4. When heat treated at 900 ℃, the W NPs itself displays a Tafel slope of 156 mV/decand an overpotential of 295 mV at a current density of 10 mA/cm^2. Heat treatment at 1000℃,1450℃, and 1150℃ produced W_2C/WC thin films, which each have the overpotential values of 389 mV, 384 mV, and 310 mV, respectively. As a rule of thumb, lower overpotential indicates a better HER performance. Therefore, it can be concluded that the W_2C/WC thin film heat treated at 1150℃ is the best candidate compared to the other thin films. The Tafel slope for this material is 108 mV/dec. **Figure 2.10** shows the Tafel slope obtained from the study.

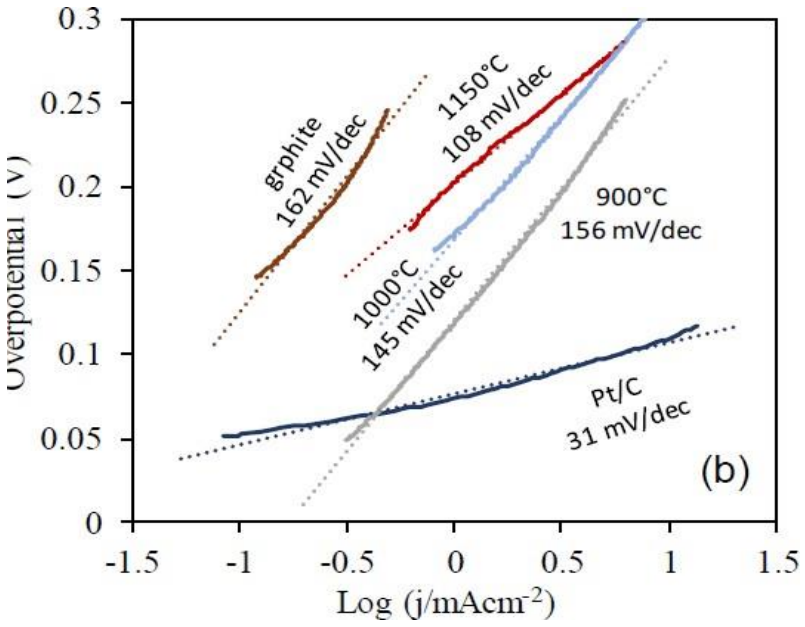

Figure 2.10 Tafel plots of graphite, Pt/C and W_2C/WC thin film heat treated at temperatures of 1150,1000 and 900℃ (Emin et al, 2018)

As a stand-alone electrocatalyst, WC displays a higher HER performance in comparison with W_2C, WO_3, and WO_2 (Harnisch, Sievers, and Schroder, 2009). In the study, the maximum current density obtained at an acidic condition is – 118 mA/cm^2 at an overpotential of 760 mV and 26 mA/cm^2 at an overpotential of 300 mV. In a neutral pH and at an overpotential of 300 mV, 8.8 mA/cm^2 of current density is obtained.

2.2.2.2) W-based Oxides

Due to being enriched with varying crystalline phases and adjustable composition modulation, there is a high probability for tungsten oxide to attain adequate catalytic activity, either by crystal structure engineering or surface electronic state modulation (Chen etal, 2021). Chen et al also point out three strategies for enhancing the HER activity for tungsten oxides, namely controlling the surface morphology, engineering defects and synergistic catalysis.

For morphology control, one best example for each structure is from a study by Liu et al(2017), Nayak et al (2017), and Ma et al (2019). Each of these studies employs three different structures for the tungsten oxides, 1D, 2D and 3D respectively. The 1D structure involves the nanostructures, such as nanowires (Chen et al, 2021). Liu et al (2017) synthesize ultra-long 1D nanowires with a rough surface through the calcination of W-polydopamine precursors. The electrolyte used for the test was 0.5M H_2SO_4. The material obtained displays an overpotential of 108 mV at 10 mA/cm^2, with a Tafel slope of 46 mV/dec, as shown in **Figure 2.11**.

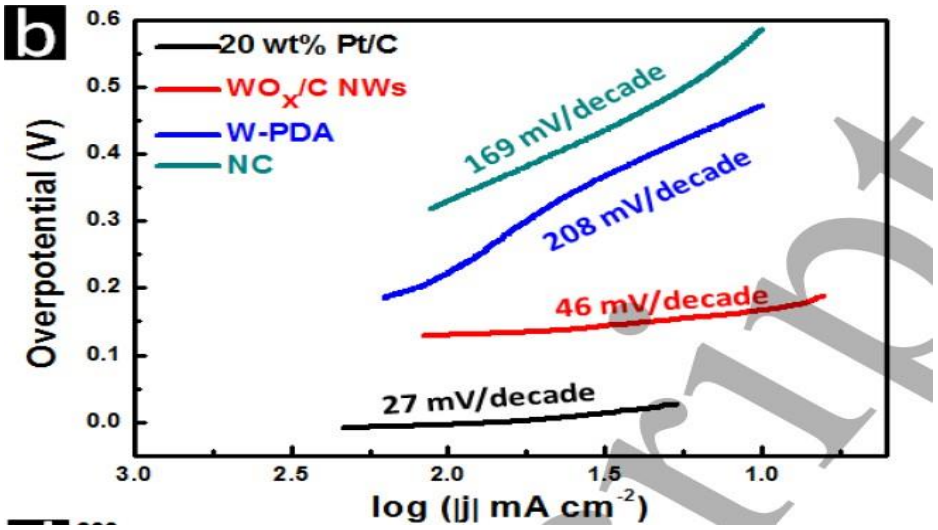

Figure 2.11 The Tafel plots for 20 wt% Pt/C, WO_x/C NWs, W-PDA, NC (Liu et al, 2017)

2D structure possessed exposed specific crystal planes which supply a large electron-electrolyte interface, enabling the process to be conducted effortlessly (Xie et al, 2012). A study by Nayak et al (2017), which involves the utilization of square-shaped stacked WO3 nanoplates tested in a 1M H_2SO_4 electrolyte displays an overpotential of 73 mV in 10 mA/cm^2, and a Tafel slope of 40 mV/dec. The Tafel plots are illustrated on **Figure 2.12**.

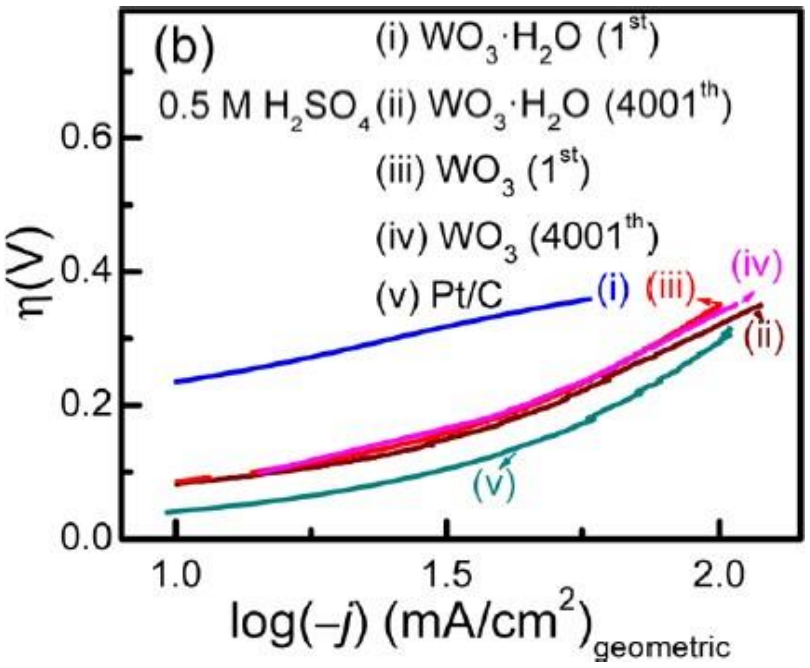

Figure 2.12 Tafel plots of $WO_3 \cdot H2O$, WO_3 & Pt/C (Nayak et al, 2017)

For the 3D structure, high-efficiency anisotropic electron transfers usually occurred on the catalyst surface (Chen et al, 2021). Ma et al (2019) synthesized Ag-WO3 core-shell nanostructures, which display an overpotential of 207 mV at 10 mA/cm^2 with the Tafel slope of 52 mV/decwhen tested in a 0.5M H_2SO_4 electrolyte. **Figure 2.13** shows the Tafel plots of the study.

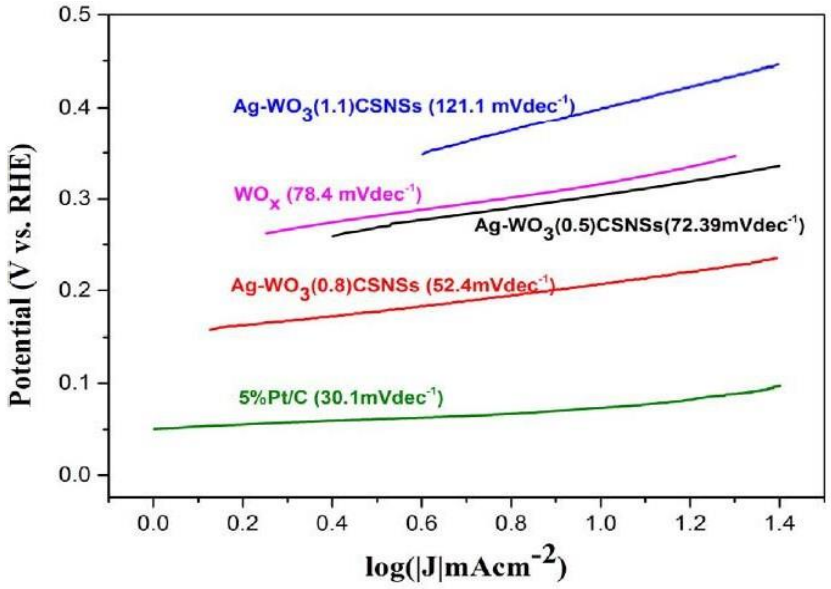

Figure 2.13 Tafel plots of WO_x, Ag·WO_3(1.1)CSNSs, Ag-WO_3, Ag·WO_3(0.8)CSNSs, 5% Pt/C (Ma et al, 2019)

Defect construction involves the modifications of the electronic structure of both the oxygen and tungsten sites on the catalyst to activate the reaction sites (Chen et al, 2021). In this case, a suitable example would be the study by Sharma, Kumar & Hader (2019). The study involves the utilization of Vac-WO_{3-x}, which is a tungsten oxide possessing oxygen vacancies and undergoes a structural alteration from the hexagonal to monoclinic phase. This material then undergoes a heat treatment at 550℃. As a result, the Tafel slope obtained is 30 mV/dec, while the overpotential is 55 mV at 1 mA/cm^2. Shown in **Figure 2.14** are the Tafel plotsof Vac-WO_{3-x}.

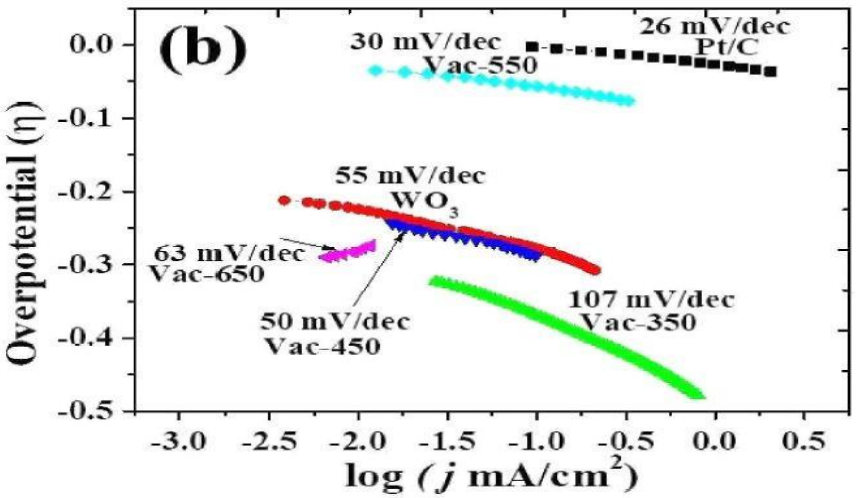

Figure 2.14 Tafel plots of Vac-WO_{3-x}, Pt/C, WO_3 & various Vacs (Sharma, Kumar & Hader, 2019)

For synergistic catalysis or more particularly confined catalysis, the carbon materials act as a protective layer for the catalyst to prevent corrosion, trigger a unique catalytic activity and enhance its durability (Yu, Deng & Bao, 2020). Jing et al (2019) utilized a carbon-encased WO_x on carbon support (WO_X@C/C), where the carbon encasement serves as the electron acceptor/donor and enhances the conductivity. In 0.5M H_2SO_4 electrolyte, the material displays an overpotential of 36 mV at 60 mA/cm^2 with a Tafel slope of 29 mV/dec, as illustrated in **Figure 2.15**.

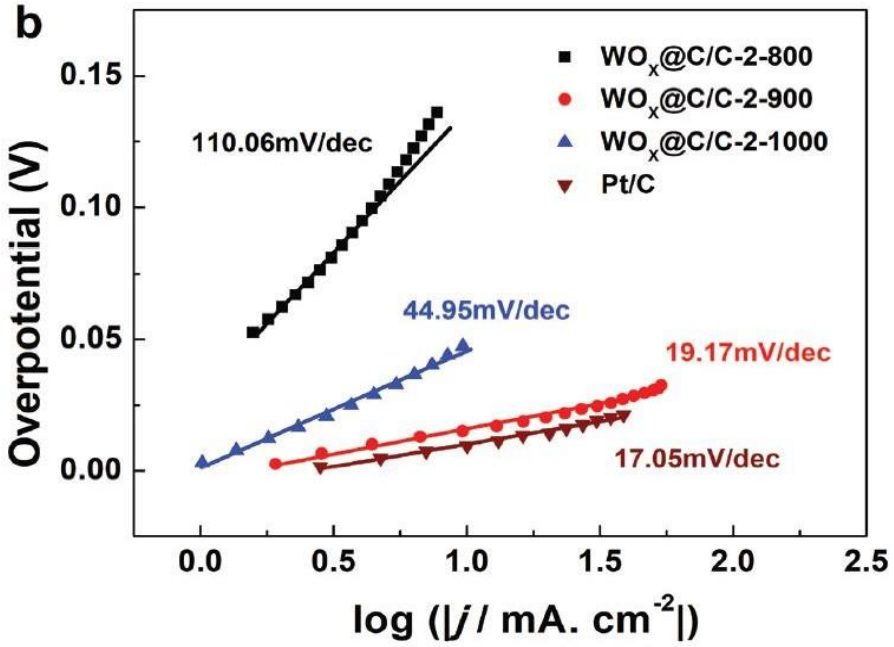

Figure 2.15 Tafel plots of Pt/C and variations of WO_X@C/C (Jing et al, 2019)

2.2.2.3) W-based Sulphides

Similar to MoS_2, WS_2 have electrocatalytically inert basal planes (Tan & Pumera, 2016).In the study, Tan & Pumera utilized a mixture of WS_2/WS_3 film-like material which undergoes electrosynthesis to produce $WS_{2.64.}$ This material exhibits an overpotential of 494 mV at -10 mA/cm^2. For comparison, WS_2 has the worst overpotential, valuing 652 mV at a similar current density. $WS_{2.64}$ display a Tafel slope of 43.7 mV/dec. The plots of $WS_{2.64}$ in comparison with other materials is illustrated as **Figure 2.16**.

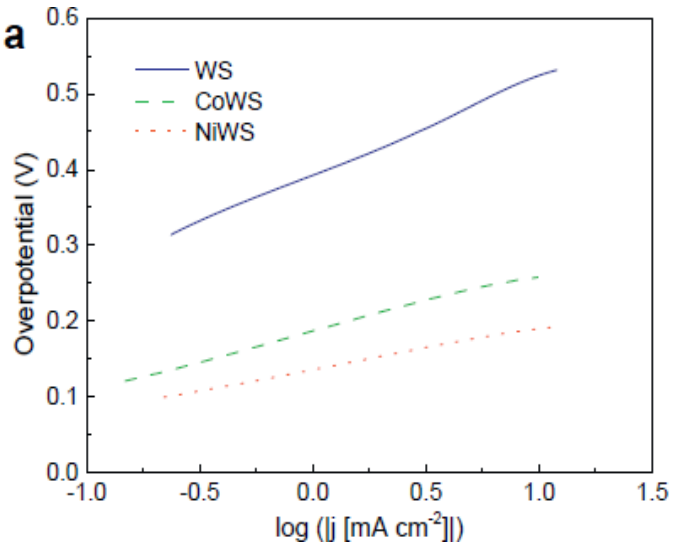

Figure 2.16 Tafel slopes of $WS_{2.64}$ in comparison with Pt/C, bare GC, & other variations of WS (Tan & Pumera, 2016)

In a study by Yang et al (2015), Ni and Co were used as a dopant for amorphous tungsten sulphide to improve the tungsten HER activity. In 0.5 M H_2SO_4, a dopant to W ratio being 1:3, and heat treatment at 210℃, the overpotentials for both materials, CoWS and NiWS, are 330 mV and 265 mV respectively. As a comparison, amorphous WS_x displays an overpotential of 604 mV, indicating a considerable enhancement in HER activity in terms of overpotential through doping. The Tafel slopes obtained are 129 mV, 55 mV, and 74 mV for amorphous WSx, NiWS, and CoWS respectively. As lower overpotential and Tafel slope indicate better HER performance, it can be concluded that nickel doping resulted in the best HER activity compared to the other two materials. **Figure 2.17** illustrates the Tafel plots of the materials.

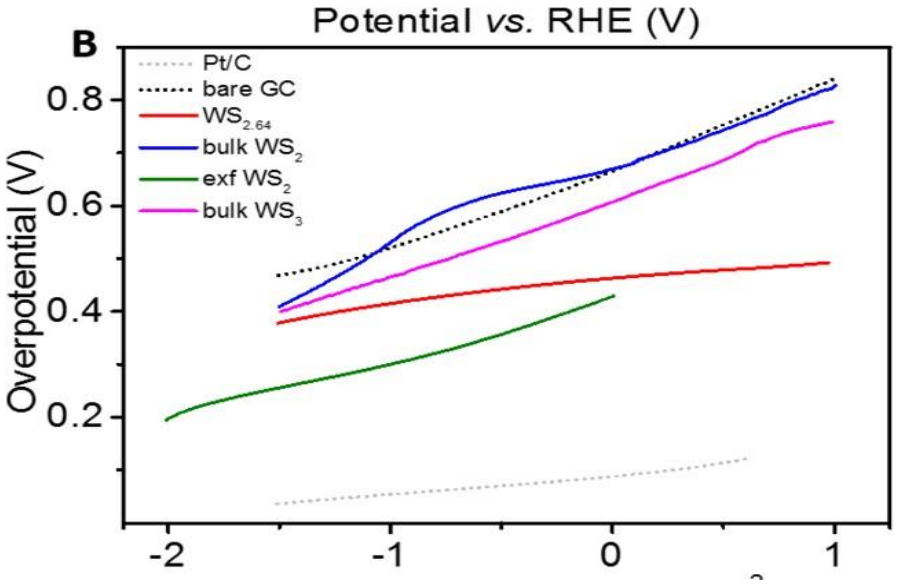

Figure 2.17 Tafel plots of WS, CoWS and NiWS (Yang et al, 2015)

Other methods of enhancement include defect engineering and phase transition (Ni et al, 2020). According to Ni et al, the introduction of defects could maximise the available active sites and improve the catalytic activity. Ling et al (2018) develops a defect-rich tungsten disulphide through partial sulphurisation of tungsten oxide to produce WS_2/WO_3 nanosheets. An alkaline solution eliminates the WO_3 template, causing pores and additional edge defects to develop. The precursor undergoes complete thermal decomposition at a temperature of 450℃ to form WS_2. The final product displays an 145 mV of overpotential at 10 mA/cm^2, with the Tafel slope valuing at 58.5 mV/dec, as shown in **Figure 2.18**.

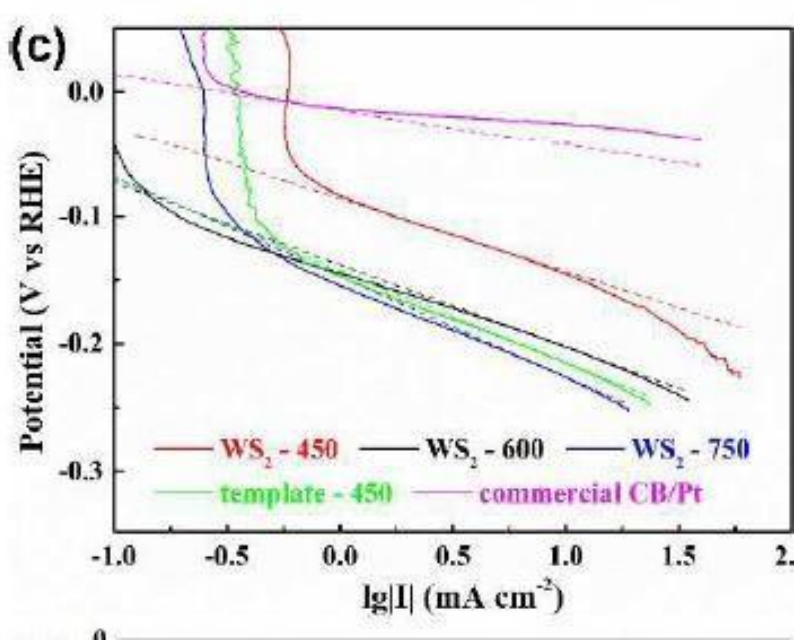

Figure 2.18 Tafel plots of various WS_2 and commercial CB/Pt (Ling et al, 2018)

As for phase transition, a study by Liu et al (2018) describes the synthesis of a 1T' phase WS_2 nanoparticles with 2H phase WS_2 nanostructures through an effective colloidal synthesis strategy. The reaction between WS_2- and the positively charged surfactant significantly stabilizes the 1T'-WS_2, enabling dispersion of the material in a polar solvent. The material itself exhibits an overpotential of 200 mV and 50.4 mV/dec as the Tafel slope, as shown in **Figure 2.19**.

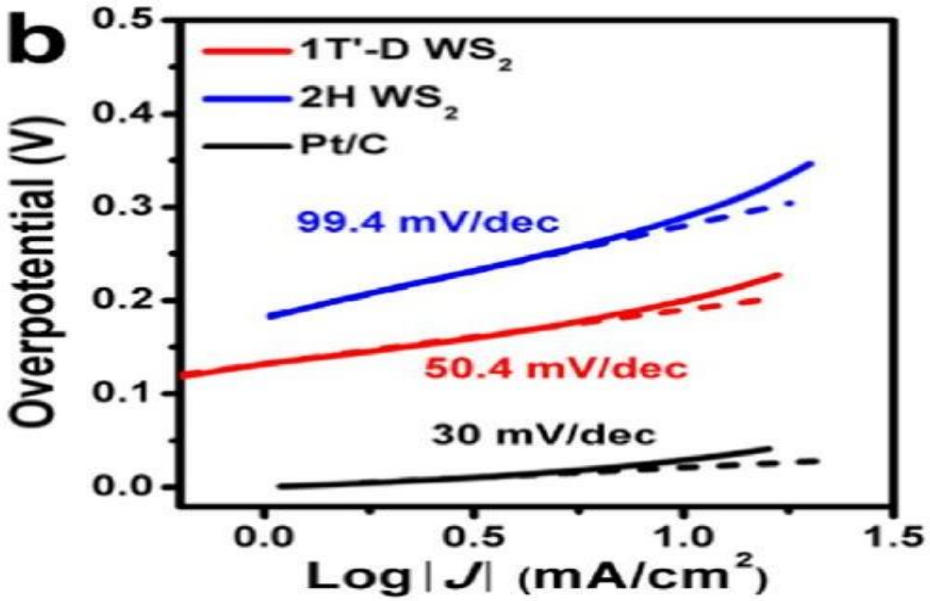

Figure 2.19 Tafel plots of Pt/C, 2H phase WS_2, and 1T' phase WS_2 nanoparticles (Liu et al, 2018)

2.3) Simulation of HER

A simulation could be utilized for HER to determine the electrocatalytic properties and the mechanisms of the reaction, and the optimization of the reaction. For example, Lofti et al (2019) utilize a response surface methodology (RSM) procedure to study the characterization of HER on porous Ni/Cu electrodes and to enhance and optimize operations through a collection of mathematical and statistical methodologies. RSM was applied to study the effects of varying concentrations of $(NH_4)_2SO_4$, composition ratio for Ni/Cu, and the settling time while the optimization of these parameters will be conducted with the application of central composite design (CCD) approach. For the reaction, the conditions are as follows: 2 A/cm^2 of current density, 1 pH level, and a 298 K as the temperature.

From the simulation, it is found that a 0.02 M $(NH_4)_2SO_4$, 48.3 as the Ni/Cu ratio, and a 4.8 min of settling time provided the optimum condition for the reaction. Furthermore, the optimum overpotential obtained is 203 mV at 10 mA/cm^2 while the Tafel slope displayed is 88.2 mV/dec. In comparison, the study also shows that Ni foam displays a Tafel slope of 147 mV/dec. The simulation also reveals the active sites' area for Ni/Cu is about 1790 cm^2.

2.4) Applications of Electrocatalysts

2.4.1) Energy Storage

Some examples of energy storage include the Li-ion battery and metal-air batteries, and ammonia production (Wang et al, 2017). For an application in energy storage, electrocatalysts are developed for electrochemical reductions of water, carbon dioxide, and nitrogen, which occur at the cathode in electrolysis (DuBois, 2014). DuBois also explains that the improvement of efficiencies of an electrocatalyst in both anodic and cathodic reactions is compulsory to prevent excessive loss of energy. According to Wang et al (2017), the reduction of overpotential is compulsory in developing an energy storage system with great electricity- in/electricity-out efficiency which is made possible by electrocatalyst.

The most promising among these applications would be the metal-air batteries due to its great theoretical energy density (Tahir et al, 2017). The study also describes the challenges faced in utilizing metal-air batteries. They are low power generated, poor cyclic life, and poor round-trip efficiency. According to Tahir et al, its reversibility is dependent on the efficiency of the OER, which itself influenced by the cathode catalytic activity. The authors also states that the catalytic activity reverses the process and maintains a clear air pathway for the next cycle through the consumption of solid products by oxygen evolution reaction. Similar to HER, the most efficient catalyst for OER is the noble-metal-based catalyst, such as Pt, which itself is not economically sustainable due to high costs and scarcity.

2.4.2) Fuel Cells

Fuel cells mechanism that utilizes catalytic oxidation of fuel for conversion of electrical energy from chemical energy, with the most popular being the reversible fuel cells and solid oxides owing to their fuel resurge and storage for energy, respectively (Tahir et al, 2017). In terms of energy generation, hydrogen fuel cells are more beneficial compared to combustion-based technologies as the energy conversion is higher than combustion engines, and it is regarded as a cleaner alternative for fuel due to zero carbon emissions.

The electrodes of the fuel cells comprise porous material enclosed in a layer of catalyst. At the anode, the molecular hydrogen supplied by a gas-flow stream is oxidized

and produced hydrogen ions and electrons. As the electrons travel from the cathode to the external circuit, the ions are delivered to the electrolyte. The supplied oxygenreacts with the electrons and the protons to form water at the cathode. Below is the overall reaction to the process (Sharaf & Orhan, 2014):

$$H_2 + \frac{1}{2}O_2 \rightarrow H_2O + W_{ele} + Q_{heat} \qquad \text{(Eq. 2.7)}$$

According to Sharaf & Orhan (2014), the main obsatacles for the global utilization of fuel cells are high costs, low durability, and lack of codes and standards to convince the authority, business leaders and the public regarding its safety features and for a continuous ideal power generation, heat and water by-products are required to be perpetually removed.

2.5) Chapter Summary

HER is one of the main reactions in water electrolysis. The reaction itself comprises 3 steps: Volmer, Tafel & Heyrovsky step. The proton adsorption at the electrocatalyst surface occurs during the Volmer step. For the Tafel and Heyrovsky reaction, the discharging of hydrogen from the electrocatalyst surface, in an electrochemical and chemical manner respectively. Besides hydrogen production via electrolysis, electrocatalysts are also applicable as fuel cells and energy storage. Other than Mo, W is also a comparable alternative for Pt electrocatalyst. **Tables 2.1** & **2.2** summarized the performance of both electrocatalysts.

Table 2.1 Performance of various Mo-based electrocatalyst

Materials	**Overpotential (mV)**	**Tafel slope (mV/dec)**	**Exchange Current Density (mA/ cm^2)**
MoS_2 film	-	120	2.2E-03
Ni-MoS_2	98	-	10
MoS_2(S180)	120	55	-
MoS_2 with V-doped interlayer	130	69	-
$MoSe_{2-x}$	170	98	-
S-doped $MoSe_2$	156	58	30
N-doped $MoSe_2$	98	49	-
N-$MoSe_2$/TiC-C	137	32	100
Amorphous $MoSe_a$	270	60	10
np-Mo_2C NW-modified GCE	200	-	60
np-Mo_2C NW-modified GCE combined with Vulcan carbon	200	54	80
γ-MoC	270 - 310	121.6	3.2
Fe-doped β-Mo_2C	-140	-	-0.15 – -0.25

Table 2.2 Performance of various W-based electrocatalyst

Materials	**Overpotential (mV)**	**Tafel slope (mV/dec)**	**Exchange Current Density (mA/ cm^2)**
W_2C/WC thin film (heat treated at 1150℃)	310	108	10
WC	760 (Acidic)	-	118
	300 (Acidic)	-	26
	300 (Neutral)	-	8.8
WOx nanowires	108	46	10
WO3 nanoplates	73	40	10
Ag-WO3	52	52	10
Vac-WO3-x	55	30	1
WO_X@C/C	36	29	60
$WS_{2.64}$	494	43.7	-10
NiWS	265	55	-
WS2-450	145	58.5	10
1T'-WS_2	200	20.4	10

Chapter 3 Methodology

3.1) Overview

The project's methods will be covered in this chapter. This comprises the general study plan, the tool used, the processes, the technique for gathering data, and the data analysis.

3.2) Research Strategy

In this project, simulation software will be used to evaluate the HER performance of MoS_2 and $MoSe_2$. The simulation will also include the same modifications on the electrocatalyst surface as Kong et al. (2013). Its performance will be analyzed based on its overpotentials, current densities, and Tafel slope using the Volmer-Heyrovsky-Tafel mechanism. From the simulation, the VHT mechanistic steps can be determined and also the validity of the literature can be proven. **Figure 3.1** below illustrates the flow chart for this research.

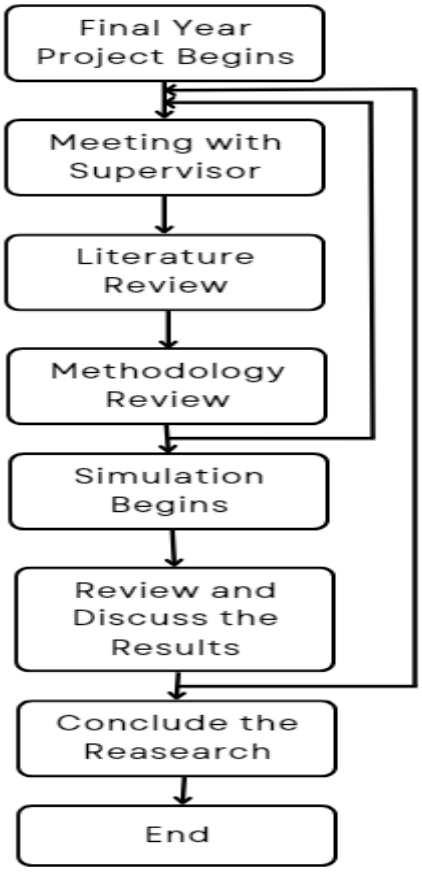

Figure 3.1 Flowchart of the Research

3.3) Research Approach

Based on the literature reviewed, the MoS_2 and $MoSe_2$ will be chosen as the electrocatalyst for the simulation. The simulation aims to determine the electrocatalytic properties of the chosen electrocatalysts, compare their properties with those of Pt-based, and validate the results obtained by Kong et al (2013). Similar to the study, the simulation will be conducted in an acidic condition of 0.5 M H2SO4.

Assuming the Langmuir adsorption isotherm is valid, the rate for Volmer, Heyrovskyand Tafel reactions are:

$$Volmer: v_V = k_V^0 c_{H^+}(0)\Gamma_\infty(1 - \theta_H)e^{-\beta_V f(E - E_V^0)}$$

$$Heyrovsky: v_H = k_H^0 c_{H^+}(0)\theta_H \Gamma_\infty e^{-\beta_H f(E - E_H^0)}$$

$$Tafel: v_T = (k_T^0 \Gamma_\infty^2)\theta_H^2$$

The parameters v_i are the reaction rate with a unit of mol/cm^2 s, k_i^0 are the

concentration-independent forward reaction rate constants, Γ_∞ is the surface coverage correlate to the adsorption sites available, $C_H^+(0)$ are the surface concentration of H^+, $C_{H^2}(0)$ are the surface hydrogen concentration in mol/cm^3, β_i are the symmetry coefficients for Volmer and Heyrovsky steps, E_i^0 are the standard potentials for Volmer and Heyrovsky steps, and $\Theta_H = \Gamma_H/\Gamma_\infty$ is the surface coverage by adsorbed hydrogen.

3.4) Data Collection Method and Tools

The simulation software COMSOL Multiphysics, which is a finite element-based modelling software, is chosen to analyze the HER activity of the selected electrocatalysts. For this study, COMSOL Multiphysics version 5.5 will be used to conduct the simulation.

Model Builder and Application Builder are the two primary parts of COMSOL Multiphysics. The Model Builder is used to define the model and its elements, and the Application Builder allows for the rapid generation of applications with a particular user interface based on the model produced there (COMSOL, 2019). The Model Builder will serve as the study's focus.

Figure 3.2 is the graphical user interface (GUI) of the COMSOL Multiphysics with Model Builder. **Table 3.1** lists the components of the (GUI) along with its description.

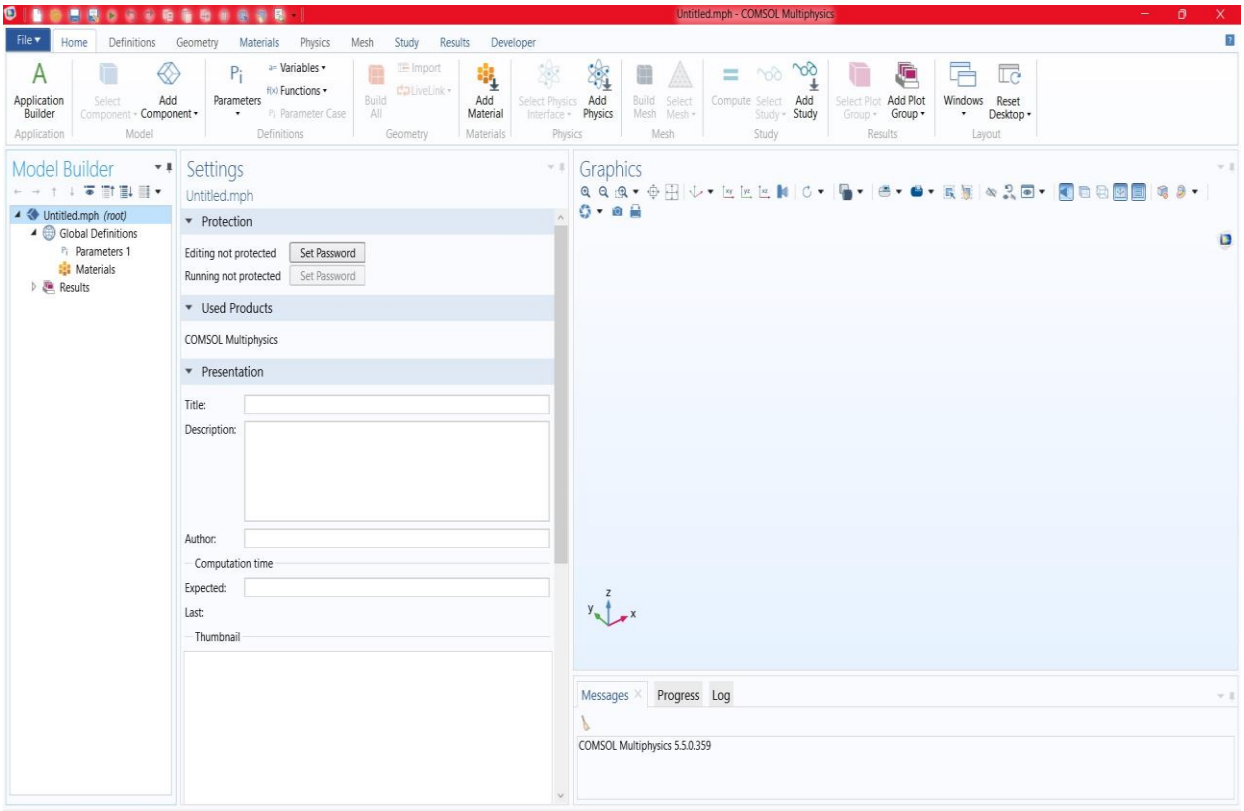

Figure 3.2 COMSOL Multiphysics Model Builder GUI

Table 3.1 Components of COMSOL Multiphysics Model Builder GUI

Component	Description
Application Builder	To switch to the Application Builder
Model Tree	Gives a general summary of the model's features, operations, and construction processes.
Model Builder Window	Shows the model tree and the toolbar buttons
Quick Access Toolbar	To access functionality such as saving and opening
Ribbon	Have the buttons and drop-down lists for controlling all steps in the modelling
Settings Window	Provides settings of the chosen node in the model tree
Graphic Window	Illustrates the interactive graphics for the Geometry, Mesh, and Results nodes. Also enables rotating, panning, zooming, and selection
Information Window	Shows the display vital model information during the simulation. This includes solution time, solution progress, and results tables

A model can be generated either through the Model Wizard or Blank Model button as shown in **Figure 3.3** below.

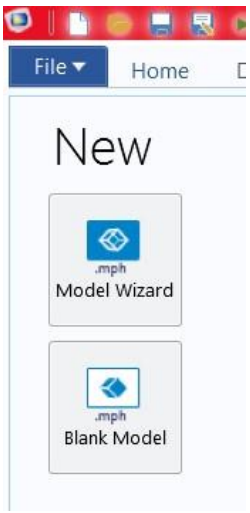

Figure 3.3 Model Buttons

The first step in generating a model guided by the Model Wizard is the selection of space dimension for the model. The selections include 0D, 1D Axisymmetric, 2D, 2D Axisymmetric, and 3D as shown in **Figure 3.4**.

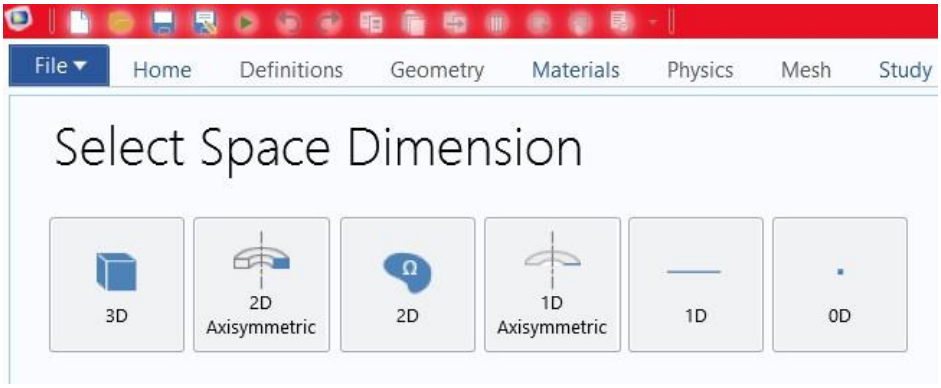

Figure 3.4 Space Dimension Buttons

This is followed by the selection of one or more physics interface. **Figure 3.5** shows the available physics interface in COMSOL Multiphysics version 5.5.

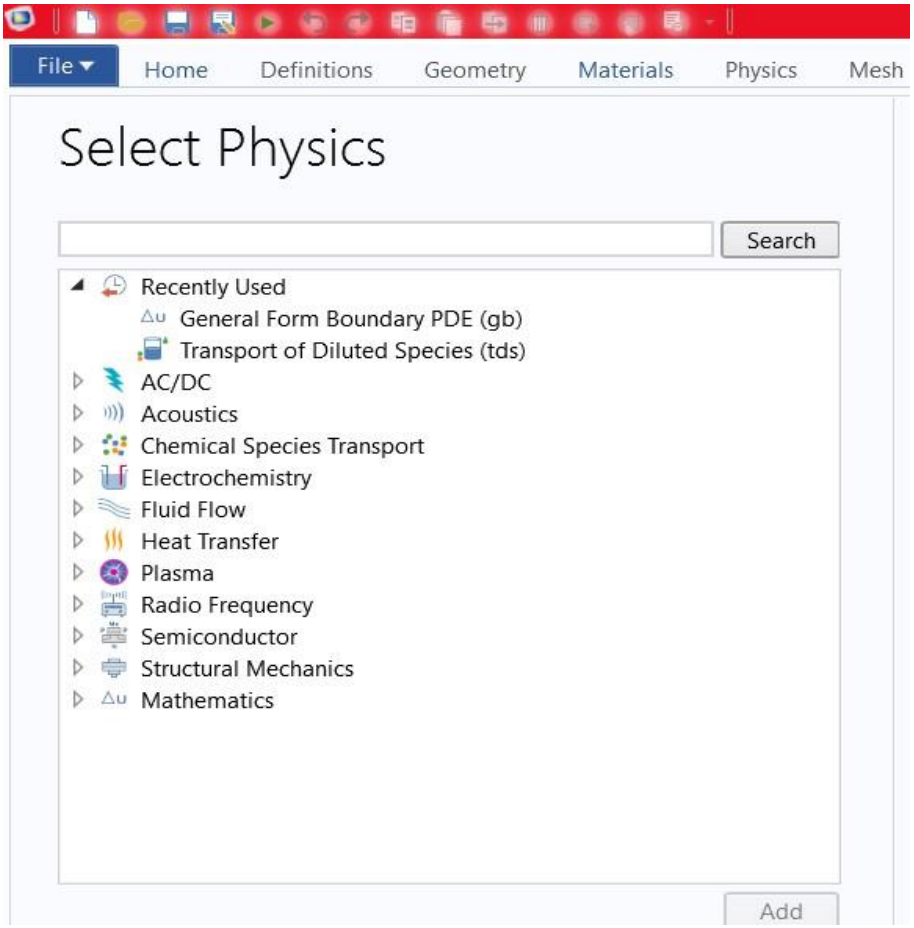

Figure 3.5 Physics Interfaces

Lastly, is the selection of study type, which is the solver(s) necessary for the computation. **Figure 3.6** shows the study type available in the software.

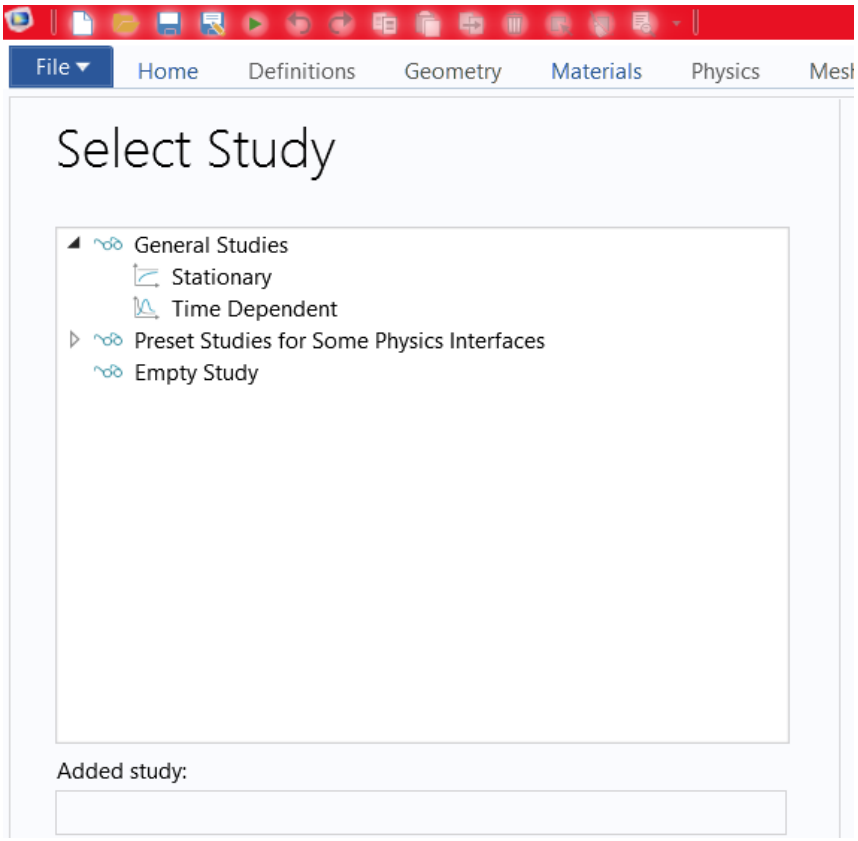

Figure 3.6 Study Type

As for Blank Model, the software interface will be absent of Components and Study. Instead, both are added manually through right clicking the model tree. For this project, the model will be generated by the Model Wizard.

3.5) Simulation Procedures

Here are the steps involved in developing the model and simulation.

1) COMSOL Multiphysics is launched.
2) Model Wizard is selected.
3) 1D is selected for the Space Dimension.
4) Transport of Diluted Species (tds) and General Form Boundary PDE (gb) were selected for the Physics interface.
5) Time Dependent is selected as the Study type.
6) The parameters in the Parameters node are filled as in **Table 3.2**

Table 3.2 Simulation Parameters

Parameters	Values	Unit	Description
F	96485.33	C/mol	Faraday's Constant
R	8.314	J/(mol*K)	Gas Constant
T	298.15	K	Temperature
α_V	1 - β_v	-	Transfer Coefficient for Volmer Step
α_H	1 - β_h	-	Transfer Coefficient for Heyrovsky Step
E_V	0	V	Volmer's Standard Potential
E_H	0	V	Heyrovsky's Standard Potential
E_{0V}	0	V	
E_{0H}	0	V	
E_{init}	0	V	Initial Potential
C_{star}	1,000	mol/m^2	Concentration of hydrogen
G_{max}	100,000	mol/m^2	Maximum surface coverage
n	1	-	Number of electrons transferred

7) The variables in the Variables node were defined as shown in **Table 3.3**

Table 3.3 Definitions for the Variables

Name	Expression	Unit	Description
Et	abs(vb*t + Erev - Einit) + Erev	V	
Kv	kv*exp(((-Bv*n*F)/(R*T))*(Et - E0V))	$m^3/(s \cdot mol)$	
Kh	kh*exp(((-Bh*n*F)/(R*T))*(Et - E0H))	$m^3/(s \cdot mol)$	
Rv	Kv*Cstar*(Gmax-u)	$mol/(m^2 \cdot s)$	
Rh	Kh*Cstar*u	$mol/(m^2 \cdot s)$	
Rt	kt*(u^2)	$mol/(m^2 \cdot s)$	
Current	(Rv+Rh)*n*-F	A/m^2	

8) At the Transport Properties node, the velocity and the diffusion coefficient were defined as 0 m/s and 1 x 10^{-9} m^2/s, respectively.
9) At the General Form PDE node Settings window, the conservative flux, the source term, damping coefficient, and mass coefficient is defined as shown in **Figure 3.7.**

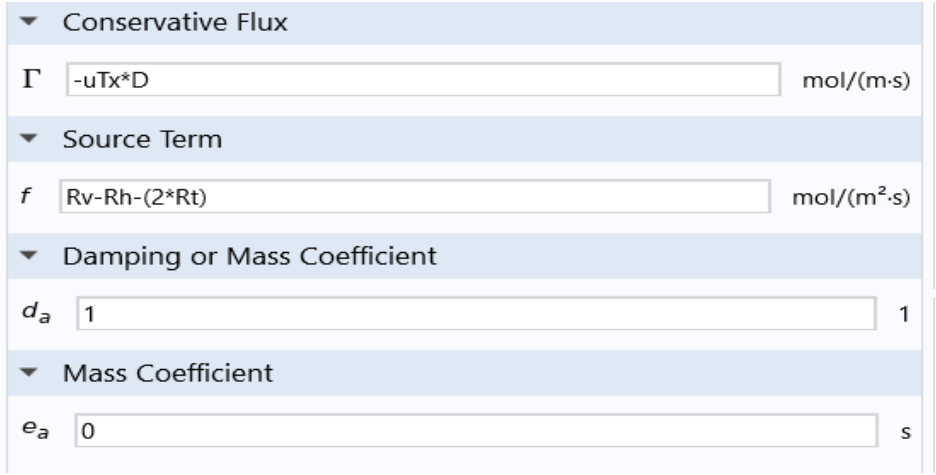

Figure 3.7 Definitions for the General Form PDE

10) The mesh is set as User-controlled.
11) At the parametric sweep, the sweep type is set as Specified combinations.
12) The k_v, k_h, β_v and β_h is set as the manipulated variables with multiple values were assigned on each of these variables.
13) At the time-dependent nodes, the time range is set to "range(0,tstep,tend)"
14) At the point graph node, the Current is set as the y-axis, and potential, Et, is set as the x-axis.
15) The computation started and the results were compared with the literature. The simulation is repeated with different values for the variables until a similar result is obtained.
16) The value of the variables that produce the desired results were recorded.
17) Another graph is created, with y-axis being the $\log_{10}$(Current) to obtain the Tafel Slope.
18) The steps were repeated to obtained results for MoS_2 and $MoSe_2$.

3.6) Chapter Summary

The simulation will be conducted using the COMSOL Multiphysics software. The materials to be tested will be MoS_2 and $MoSe_2$. The simulation will be conducted in an acidic environment of 0.5 M H_2SO_4. It is expected for both materials to display a Tafel slope at the range of 105 to 120 mV/dec. The exchange current densities are expected to be 0.0022 for MoS_2 and 0.002 for $MoSe_2$.

Chapter 4: Results and Discussion

4.1) Introduction

In this chapter, the simulation results will be introduced and discussed. The discussion will involve the comparison between the results obtained and the findings from the previous literatures, and the explanation on both results that are aligned and not aligned with the previous studies.

The value for Volmer's, Heyrovsky's and Tafel reaction rate constants, k_v , k_h, and k_t, and the symmetry coefficients for the Volmer and Heyrovsky reaction, β_v and β_h, are determined through trial and error, by using the COMSOL software. The rate constants are computed for blank, which is the carbon substrate, MoS_2, and $MoSe_2$. The chart pattern obtained will then corellated with the study by Kong et al (2013) to determine the correct value for both reaction rate constants.

4.2) Volmer-Heyrovsky Mechanisms

The results obtained were compared with the findings by Kong et al. **Figure 4.1** shows the polarization curve obtained from the study.

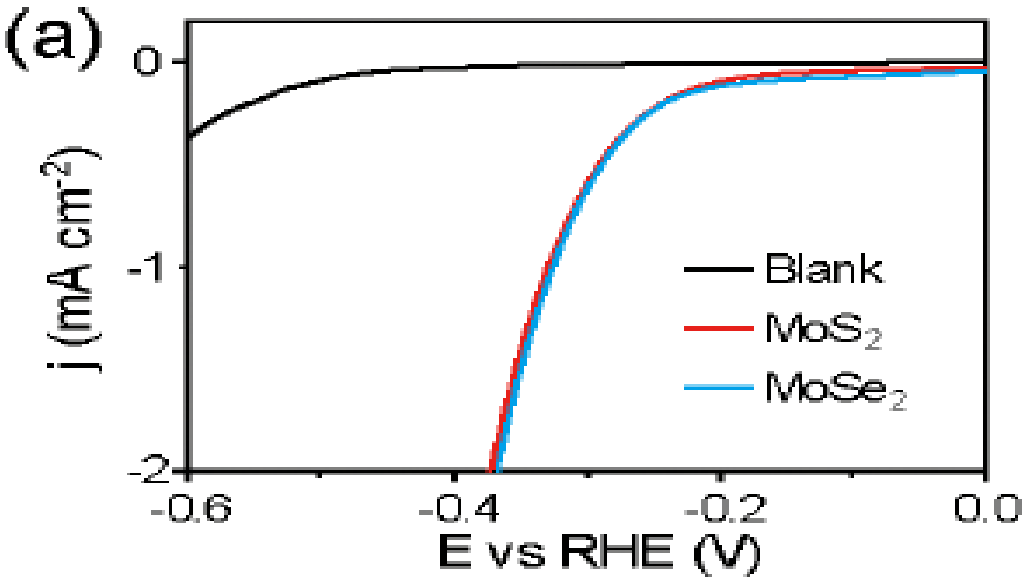

Figure 4.1 Polarization Curve of Blank, MoS_2 and $MoSe_2$ (Kong et al, 2013)

Based on the **Figure 4.1**, the current density for the blank is estimated to be -0.4 mA/cm^2 while for MoS_2 and $MoSe_2$ are both estimated to be -2 mA/cm^2. Estimation is conducted as the definite value for the current density not clearly displayed in the figure. Similarly, the reverse step potentials, E_{rev} (or E vs RHE) for MoS_2 and $MoSe_2$ were also estimated as definite values of both parameters are not given. The E_{rev} for blank is -0.6 V while E_{rev} for MoS_2 and $MoSe_2$ are estimated to be -0.38 V and -0.375, respectively.

Figure 4.2a to **c** shows the polarization curve for the blank, MoS_2, and $MoSe_2$, respectively. Each charts presents a varying value for both reaction rate constants. **Table 4.1a** to **c** show the value of both reaction constants for all three materials.

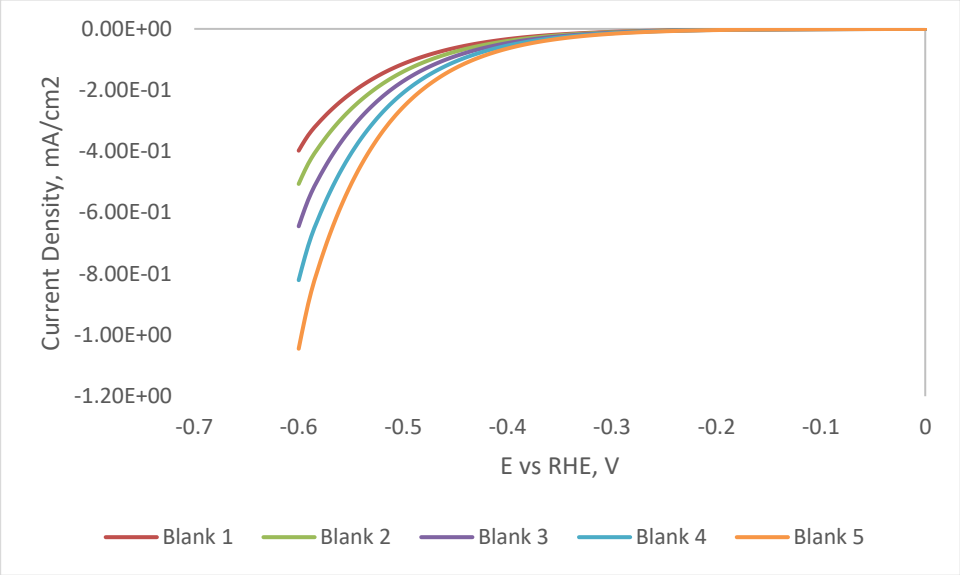

Figure 4.2a Polarization Curve of Blank

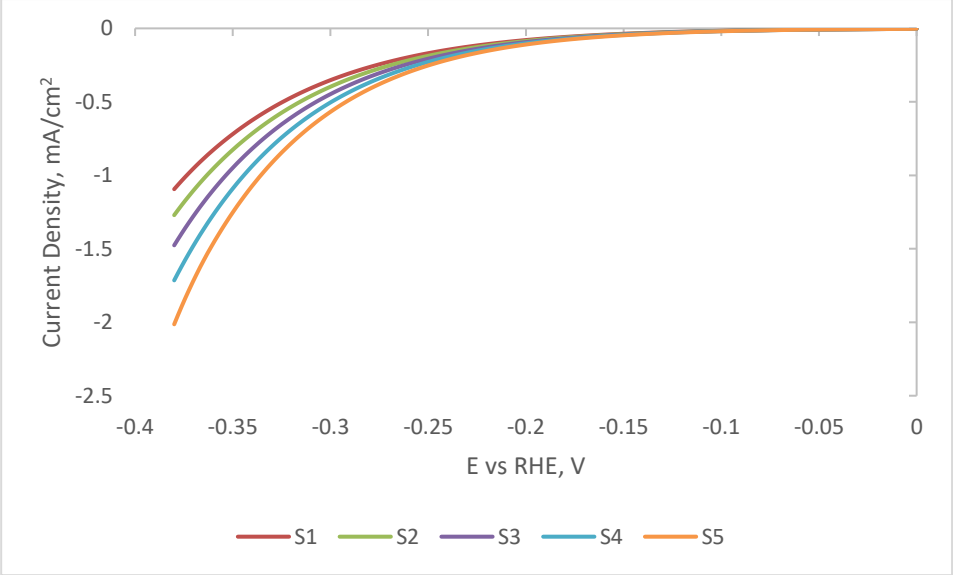

Figure 4.2b Polarization Curve of MoS_2

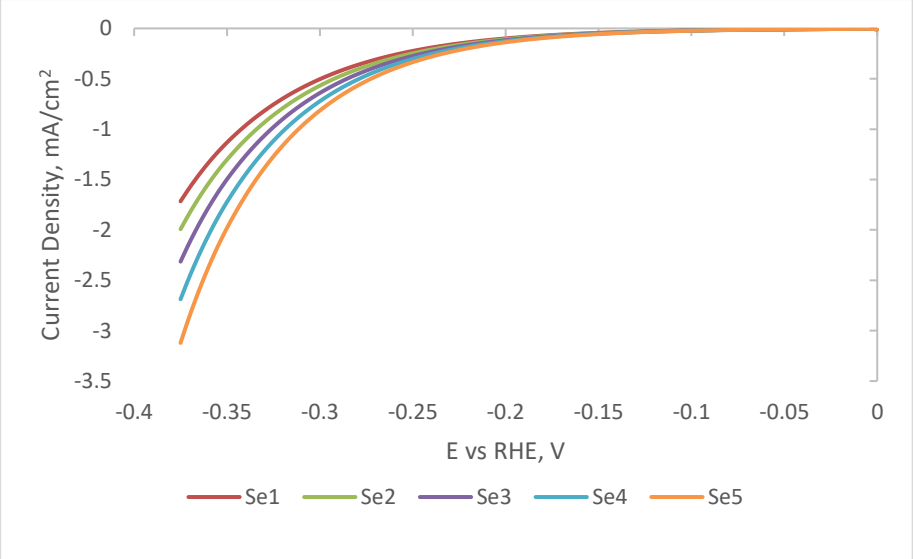

Figure 4.2c Polarization Curve of $MoSe_2$

Table 4.1a Values of Volmer's and Heyrovsky's Reaction Rate Constants for Blank

Parameters	**k_v (x 10^{-6} $m^3/(s \cdot mol)$)**	**k_h (x 10^{-6} $m^3/(s \cdot mol)$)**	**β_v**	**β_h**
Blank 1	2.96	1.46	0.46	0.31
Blank 2	2.97	1.47	0.47	0.32
Blank 3	2.98	1.48	0.48	0.33
Blank 4	2.99	1.49	0.49	0.34
Blank 5	3.00	1.50	0.50	0.35

Table 4.1b Values of Volmer's and Heyrovsky's Reaction Rate Constants for MoS_2

Parameters	**k_v (x 10^{-5} $m^3/(s \cdot mol)$)**	**k_h (x 10^{-5} $m^3/(s \cdot mol)$)**	**β_v**	**β_h**
S1	2.06	8.31	0.46	0.31
S2	2.07	8.32	0.47	0.32
S3	2.08	8.33	0.48	0.33
S4	2.09	8.34	0.49	0.34
S5	2.10	8.35	0.50	0.35

Table 4.1c Values of Volmer's and Heyrovsky's Reaction Rate Constants for $MoSe_2$

Parameters	**k_v (x 10^{-5} $m^3/(s \cdot mol)$)**	**k_h (x 10^{-5} $m^3/(s \cdot mol)$)**	**β_v**	**β_h**
Se1	9.06	2.51	0.46	0.41
Se2	9.07	2.52	0.47	0.42
Se3	9.08	2.53	0.48	0.43
Se4	9.09	2.54	0.49	0.44
Se5	9.10	2.55	0.50	0.45

From the simulation, the actual value for both reaction rate constants for all the materials were determined and tabulated in **Table 4.2**.

Table 4.2 The Reaction Rate Constants for the Materials

Materials	**k_v ($m^3/(s \cdot mol)$)**	**k_h ($m^3/(s \cdot mol)$)**	**β_v**	**β_h**	**α_v (1 - β_v)**	**α_h (1 - β_h)**
Blank	2.06 x 10^{-6}	1.46 x 10^{-6}	0.46	0.31	0.54	0.69
MoS_2	2.10 x 10^{-5}	8.35 x 10^{-5}	0.50	0.35	0.50	0.65
$MoSe_2$	9.07 x 10^{-5}	2.52 x 10^{-5}	0.47	0.42	0.53	0.58

As for the Tafel slope it is calculated using the formula:

$$b = \frac{2.3RT}{\alpha nF} \qquad \textbf{Eq. 4.1}$$

Based on the value of α on **Table 4.2** and at a temperature of 25°C, the Tafel slope for MoS_2 is displayed as 118 mV/dec while $MoSe_2$ is 111 mV/dec for the Volmer reaction. As for Heyrovsky reaction, the Tafel slope for MoS_2 and $MoSe_2$ are 90.91 mV per decade and 101.89 mV per decade, respectively. According to Bard, Faulkner and White (2022), the Tafel slope of a rate-limiting step for Volmer reaction is around 118 mV per decade, and around 40 mV per decade for Heyrovsky reaction. The given value for Tafel slope suggests

that the rate-determining step for both materials is the Volmer step, where the protons are discharged on the catalyst surface to produce hydrogen atom. **Figure 4.3** shows the Tafel plots for both these materials.

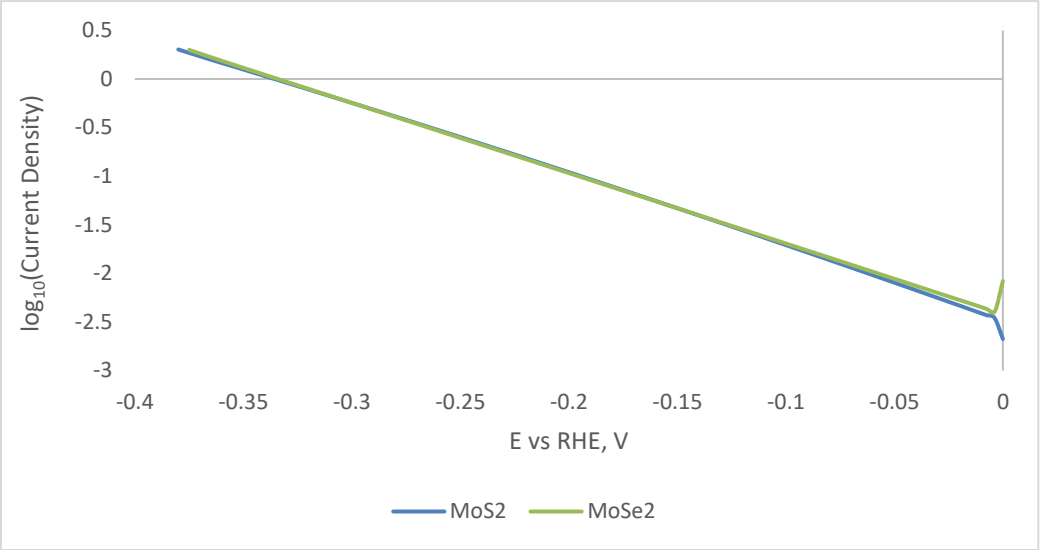

Figure 4.3 The Tafel Slope for MoS_2 and $MoSe_2$

The exchange current density, j_0, are computed by connecting the linear portion of the plots to the Tafel equation. The overpotential can be calculated using **Eq. 1.8a**. **Table 4.3** summarizes of the findings for MoS_2 and $MoSe_2$

Table 4.3 The Electrocatalytic Properties of the MoS_2 $MoSe_2$

Materials	**Exchange Current Density (mA/cm^2)**	**Tafel Slope (mV per decade)**	**Current Density (mA/cm^2)**	**Overpotentials (mV)**
MoS_2	3.47×10^{-3}	118	≈ 0.172 @ 100 mV	1.4
$MoSe_2$	3.31×10^{-3}	111	≈ 0.114 @ 100 mV	0.74

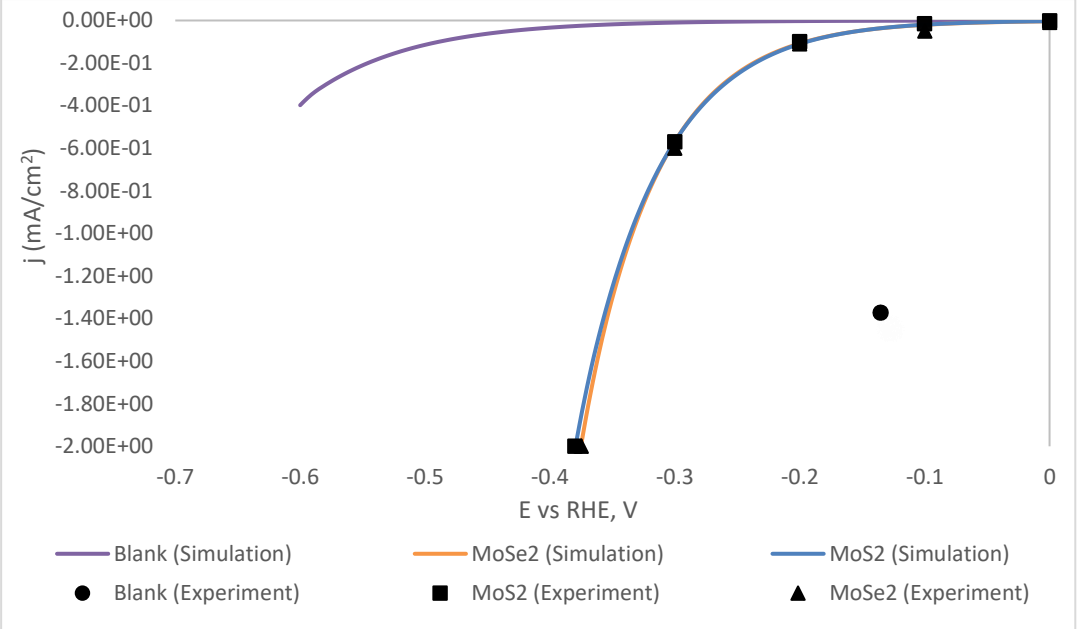

Figure 4.4 The Polarization Curve for All Materials in Comparison with the Experiment

4.3) Surface Concentration

Figure 4.5 shows the surface concentration chart of both materials against the potential. The chart describes the surface coverage by the adsorbed hydrogen on the surface of the electrocatalysts. As shown on the chart, both materials have initially displayed a small increase on the surface concentration as the potential were increased. After reaching the potentials of 3.8 x 10^{-3} V and 3.75 x 10^{-3} V for MoS_2 and $MoSe_2$, respectively, further increase in the potentials resulted in a gradual increase in the surface concentration. For MoS_2, the surface concentration experiences a gradual increase as the value of the potential is raised. As for $MoSe_2$, the surface concentration slowly increases with the potential. This indicates that the $MoSe_2$ achieves surface saturation at a faster rate compared to MoS_2.

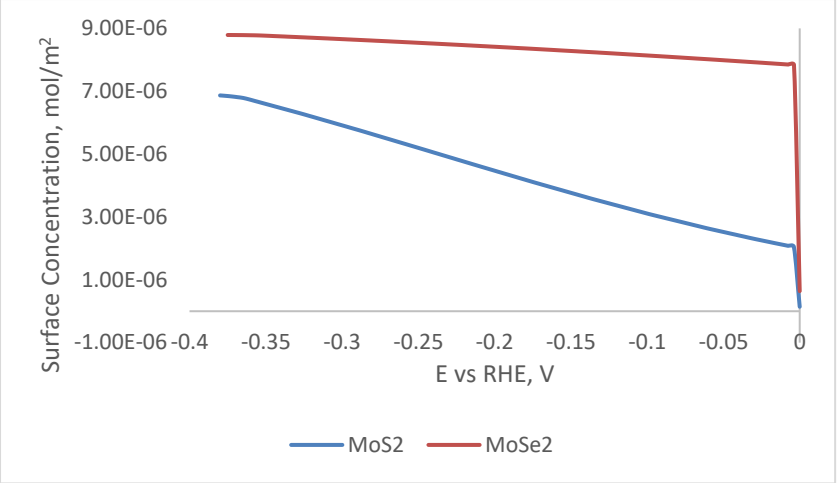

Figure 4.5 Surface Concentration of MoS_2 and $MoSe_2$

4.4) Volmer-Heyrovsky-Tafel Mechanisms

This section will discuss the effect of addition of Tafel mechanism, the desorption of two protons, into the process, with the assumption that all three reactions took place during electrocatalysis. The best fit value for MoS_2 and $MoSe_2$ were chosen and tested with varying values of Tafel reaction rate, k_T. **Figure 4.6a** and **b** shows the effect of Tafel mechanism on the Tafel plots, with **Table 4.4** serves as a legend for the varying Tafel reaction rate for the simulation.

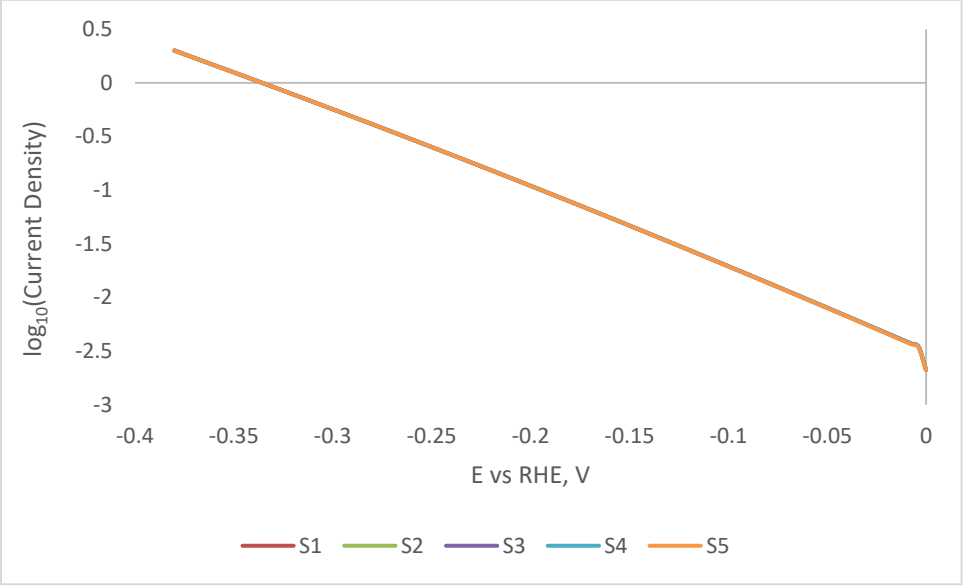

Figure 4.6a Tafel Plot of MoS_2 for VHT Mechanisms

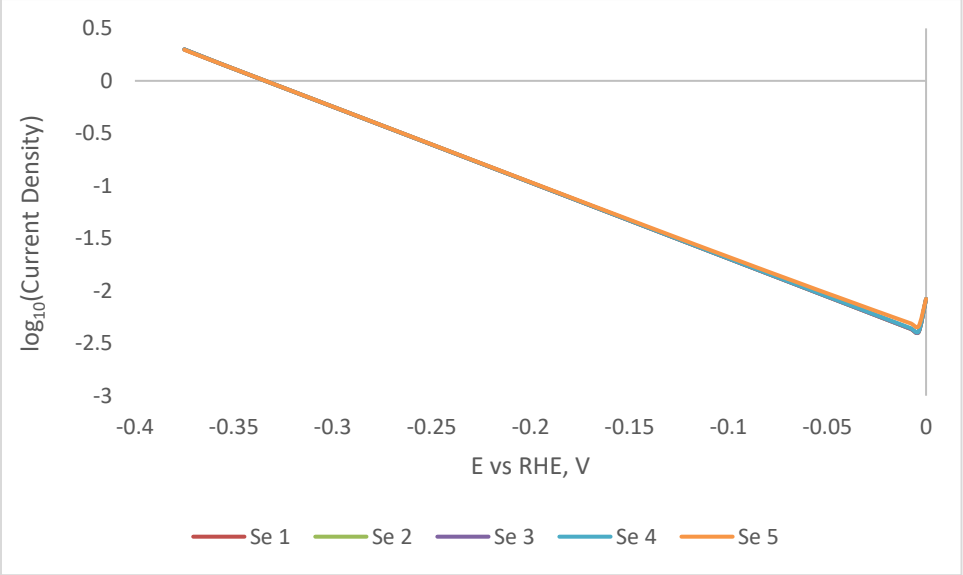

Figure 4.6b Tafel Plot of $MoSe_2$ for VHT Mechanisms

Table 4.4 The Tafel Reaction Rate Constants for the Materials

Variables	k_T (m^2/mol·s)
S/Se 1	0
S/Se 2	1
S/Se 3	10
S/Se 4	100
S/Se 5	1000

From the charts, the addition of Tafel mechanism has very little effect on the Tafel plots. Increase in Tafel plots only slightly reduce the exchange current density for MoS_2 and slightly increase the exchange current density for $MoSe_2$. The inclusion of 1000 m^2/ mol·s for Tafel reaction rate resulted in exchange current density of 3.39 and 3.80 mA/cm^2 for MoS_2 and $MoSe_2$, respectively.

4.5) Comparison with the Literature

While similar pattern is obtained for the polarization curve and the Tafel slope falls between the range of 105 to 120 mV/dec, the exchange current densities for both materials in the simulations does not corresponds to the experimental results, which is 2.2 x 10^{-3} and 2.0 x 10^{-3} mA/cm^2 for MoS_2 and $MoSe_2$, respectively. This may be due to errors in estimation for the experimental results, particularly the polarization curve of the experiment. As a result, the Tafel plots for the simulation results shifted from the experimental values, leading to different values obtained for the exchange current densities.

4.6) Chapter Summary

Trial-and-error method were utilized to determine the reaction rate constants, k, and the symmetry coefficients, β, for the materials, From the β, the transfer coefficient, α, were determined and the Tafel slope were calculated based on the α value. The Tafel slope for both materials correspond to the experimental results, while the exchange current densities were found to be greater than the experimental results, due to the error in the estimation of values for the polarization curve. $MoSe_2$ is also found to be more readily to achieve saturation and the Volmer step is the rate-determining step for both materials. It is also found that the addition of Tafel reaction on the overall process has little effect on the overall process performance.

Chapter 5: Conclusion

5.1) Conclusion

From this project, it can be concluded that:

- For MoS_2, the Tafel slope, the overpotential and the exchange current density are 118 mV per decade, 1.4 mV, and 3.47 x 10^{-3} mA/cm^2, respectively. While for $MoSe_2$, the values for these parameters are 111 mV per decade, 0.74 mV, and 3.31 x 10^{-3} mA/cm^2, respectively.
- The Tafel slope for both materials correspond to the experiment results but not the exchange current density as it is higher than the experimental results. Therefore, a more accurate estimation from the experimental polarization curves is required to reduce the error in the simulation.
- The simulation also shows that the Volmer step is the rate-limiting reaction for both materials.
- $MoSe_2$ achieves saturation at a faster rate than MoS_2.
- The addition of Tafel reaction in the overall process has little effect on the performance.
- In comparison with Pt, both MoS_2 and $MoSe_2$ would not be a suitable substitute for Pt as the Tafel slopes are significantly higher than Pt.

5.2) Recommendations

By modifying the material's surface, it is possible to increase the active sites and improve the performance of metals as electrocatalysts for HER. A modification of this kind could decrease the overpotential and the Tafel slope and increase the exchange current density, as demonstrated by the literature and simulation. A simulation could be conducted not only to validate the results from previous studies but also to determine other parameters that are not included in the literature. As an example, this simulation also reveals the surface concentration between both materials, which help in determining the degree of saturation between MoS_2 and $MoSe_2$ and helps in computing the overpotentials.

References

1 Bae, S.-Y., Jeon, I.-Y., Mahmood, J., & Baek, J.-B. (2018). Molybdenum-Based Carbon Hybrid Materials to Enhance the Hydrogen Evolution Reaction. *Chemistry - A European Journal.* DOI:10.1002/chem.201804140

2 Bard, A. J., Faulkner, L. R., & White, H. S. (2022) *Electrochemical Methods: Fundamentals and Applications (3rd Ed.).* Retrieved from: https://cloudflare-ipfs.com/ipfs/bafykbzacedeng3iagxxlxxgc3wnw6bv4opzllgtv4363j3b2woz56wbzrwa3u?filename=Allen%20J.%20Bard_%20Larry%20R.%20Faulkner_%20Henry%20S.%20White%20-%20Electrochemical%20Methods_%20Fundamentals%20and%20Applications-Wiley%20%282022%29.pdf

3 Chen, X., Yang, J., Cao, Y., Kong, L., & Huang, J. (2021). Design Principles for Tungsten Oxide Electrocatalysts for Water Splitting. *ChemElectroChem, 8(23),* Pp. 4427-4440. DOI: 10.1002/celc.202101094

4 Cho, H. H., Strezov, V., & Evans, T. J. (2022). Environmental Impact Assessment of Hydrogen Production via Steam Methane Reforming Based on Emissions Data. *Energy Reports*, *8,* Pp. 13585-13595. DOI: 10.1016/j.egyr.2022.10.053

5 COMSOL (2019). *Introduction to COMSOL Multiphysics.* Retrieved from: https://cdn.comsol.com/doc/5.5/IntroductionToCOMSOLMultiphysics.pdf

6 Deng, S., Yang, F., Zhang, Q., Zhong, Y., Zeng, Y., Lin, S., Wang, X., Lu, X., Wang, C-Z, Gu, L., Xia, X., & Tu, J. (2018). Phase Modulation of (1T-2H)-MoSe 2 /TiC-C Shell/Core Arrays via Nitrogen Doping for Highly Efficient Hydrogen Evolution Reaction. *Advanced Materials, 30(34).* DOI: 10.1002/adma.201802223

7 DuBois, D. L. (2014). Development of Molecular Electrocatalysts for Energy Storage. *Inorganic Chemistry*, *53(8),* Pp. 3935–3960. DOI:10.1021/ic4026969

8 Dubouis, N., & Grimaud, A. J. L. (2019). The Hydrogen Evolution Reaction: From Material to Interfacial Descriptors. *Chemical Science.* DOI:10.1039/c9sc03831k

9 Eftekhari, A. (2017). Electrocatalysts for Hydrogen Evolution Reaction. *International Journal of Hydrogen Energy, 42(16),* Pp. 11053–11077. DOI:10.1016/j.ijhydene.2017.02.125

10 Emin, S., Altinkaya, C., Semerci, A., Okuyucu, H., Yildiz, A., & Stefanov, P. (2018). Tungsten Carbide Electrocatalysts Prepared from Metallic Tungsten Nanoparticles for Efficient Hydrogen Evolution. *Applied Catalysis B: Environmental, (236).* Pp. 147–153. DOI:10.1016/j.apcatb.2018.05.026 35

11 Harnisch, F., Sievers, G., & Schröder, U. (2009). Tungsten Carbide as Electrocatalyst for the Hydrogen Evolution Reaction in pH Neutral Electrolyte Solutions. *Applied Catalysis B: Environmental, 89(3-4),* Pp. 455–458. DOI:10.1016/j.apcatb.2009.01.003

12 Hua, W., Sun, H.-H., Xu, F. & Wang, J.-G. (2020). A Review and Perspective on Molybdenum-Based Electrocatalysts for Hydrogen Evolution Reaction. *Nature 2020.* DOI: 10.1007/s12598-020-01384-7

13 Jing, S. Y., Lu, J. J., Yu, G. T., Yin, S. B., Luo, L., Zhang, Z. S., Ma, Y. F., Chen, W., & Shen, P. K. (2018). *Carbon-Encapsulated WO x Hybrids as Efficient Catalysts for Hydrogen Evolution. Advanced Materials, 30(28),* 1705979. DOI:10.1002/adma.201705979

14 Kong, D., Wang, H., Cha, J. J., Pasta, M., Koski, K. J., Yao, J., & Cui, Y. (2013). Synthesis of MoS2 and MoSe2 Films with Vertically Aligned Layers. *Nano Letters*, *13*(3), Pp. 1341-1347. DOI: 10.1021/nl400258t

15 Lasia, A. (2019). Mechanism and Kinetics of the Hydrogen Evolution Reaction. *International Journal of Hydrogen Energy.* DOI:10.1016/j.ijhydene.2019.05.183

16 Liao, L., Wang, S., Xiao, J., Bian, X., Zhang, Y., Scanlon, M. D., Hu, X., Tang, Y., Girault, H. H. &. Liu, B. (2013). Nanoporous Molybdenum Carbide Nanowire as an Electrocatalyst for the Hydrogen Evolution Reaction. *Energy and Environmental Science*, *3(12).* DOI: 10.1039/C3EE42441C.

17 Ling, Y., Yang, Z., Zhang, Q., Zhang, Y., Cai, W., & Cheng, H. (2018). A Self-Template Synthesis of Defect-Rich WS2 as a Highly Efficient Electrocatalyst for the Hydrogen Evolution Reaction. *Chemical Communications, 54(21),* Pp. 2631–2634. DOI:10.1039/c7cc08962g

18 Liu, C. H., Qiu, Y. Y., Xia, Y. J., Wang, F., Liu, X. C., Sun, X. H., & Liang, Q. Z. D., (2017). Noble-Metal-Free Tungsten Oxide/Carbon (WOx/C) Hybrid Nanowires for Highly Efficient Hydrogen Evolution. *Nanotechnology, 28(44),* 445403. DOI: 10.1088/1361-6528/aa8613

19 Liu, Z., Li, N., Su, C., Zhao, H., Xu, L., Yin, Z., Li, J., & Du, Y. (2018). Colloidal Synthesis of 1T' Phase Dominated WS2 Towards Endurable Electrocatalysis. *Nano Energy, 50,* Pp. 176–181. DOI:10.1016/j.nanoen.2018.05.019

20 Lotfi, N., Farahani, T. S., Yaghoubinezhad, Y., & Darband, G. B. (2019). *Simulation and characterization of hydrogen evolution reaction on porous Ni Cu electrode using surface response methodology. International Journal of Hydrogen Energy.* doi:10.1016/j.ijhydene.2019.03.208

21 Ma, J., Ma, Z., Liu, B., Wang, S., Ma, R., & Wang, C. (2019). Composition of Ag-WO3 Core-Shell Nanostructures as Efficient Electrocatalysts for Hydrogen Evolution Reaction. *Journal of Solid State Chemistry, 271*, Pp. 246-252. DOI: 10.1016/j.jssc.2018.12.020 36

22 Miao, M., Pan, J., He, T., Yan, Y., Xia, B. Y., & Wang, X. (2017). Molybdenum Carbide-Based Electrocatalysts for Hydrogen Evolution Reaction. *Chemistry - A European Journal, 23(46).* Pp. 10947 – 10961. DOI: 10.1002/chem.201701064

23 Nayak, A. K., Verma, M., Sohn, Y., Deshpande, P. A., & Pradhan, D. (2017). Highly Active Tungsten Oxide Nanoplate Electrocatalysts for the Hydrogen Evolution Reaction in Acidic and Near Neutral Electrolytes. *ACS Omega, 2(10),* Pp. 7039-7047. DOI: 10.1021/acsomega.7b01151

24 Nguyen, Q. T., Nguyen, P. D., N. Nguyen, D., Truong, Q. D., Kim Chi, T. T., Ung, T. T. D., Honma, I., Liem, N. Q., & Tran, P. D. (2018). Novel Amorphous Molybdenum Selenide as an Efficient Catalyst for Hydrogen Evolution Reaction. *ACS Applied Materials & Interfaces, 10(10).* Pp. 8659–8665. DOI:10.1021/acsami.7b18675

25 Ni, Z., Wen, H., Zhang, S., Guo, R., Su, N., Liu, X., & Liu, C. (2020). Recent Advances in Layered Tungsten Disulfide as Electrocatalyst for Water Splitting. *ChemCatChem.* DOI:10.1002/cctc.202000177

26 Pareek, A., Dom, R., Gupta, J., Chandran, J., Vivek, A., & Borse, P. H. (2020). Insights Into Renewable Hydrogen Energy: Recent Advances and Prospects. *Materials Science for Energy Technologies.* DOI:10.1016/j.mset.2019.12.002

27 Revankar, S. T. (2019*).* Nuclear Hydrogen Production. *Storage and Hybridization of Nuclear Energy*, Pp. 49–117. DOI:10.1016/b978-0-12-813975-2.00004-1

28 Sazali, N. (2020). Emerging Technologies by Hydrogen: A Review. *International Journal of Hydrogen Energy*. DOI:10.1016/j.ijhydene.2020.05.021

29 Sharaf, O. Z., & Orhan, M. F. (2014). An Overview of Fuel Cell Technology: Fundamentals and Applications. *Renewable and Sustainable Energy Reviews, 32*, Pp. 810–853. DOI:10.1016/j.rser.2014.01.012 37

30 Sharma, L., Kumar, P., & Halder, A. (2019). Phase and Vacancy Modulation in Tungsten Oxide: Study of Electrochemical Hydrogen Evolution. *ChemElectroChem.* DOI:10.1002/celc.201900666

31 Spath, P. L., & Mann, M. K. (2000). *Life Cycle Assessment of Hydrogen Production via Natural Gas Steam Reforming.* Retrieved from: https://www.osti.gov/biblio/764485

32 Sun, X., Dai, J., Guo, Y., Wu, C., Hu, F., Zhao, J., Zeng, X., & Xie, Y. (2014). Semimetallic Molybdenum Disulfide Ultrathin Nanosheets as an Efficient Electrocatalyst for Hydrogen Evolution. *Nanoscale, 6(14).* Pp. 8359-8367. DOI: 10.1039/c4nr01894j

33 Tahir, M., Pan, L., Idrees, F., Zhang, X., Wang, L., Zou, J.-J., & Wang, Z. L. (2017). Electrocatalytic Oxygen Evolution Reaction for Energy Conversion and Storage: A Comprehensive Review. *Nano Energy, 37,* Pp. 136–157. DOI:10.1016/j.nanoen.2017.05.022

34 Tan, S. M., & Pumera, M. (2016). Bottom-up Electrosynthesis of Highly Active Tungsten Sulfide (WS3–x) Films for Hydrogen Evolution. *ACS Applied Materials & Interfaces, 8(6),* Pp. 3948–3957. DOI:10.1021/acsami.5b11109

35 Vesborg, P. C. K., & Jaramillo, T. F. (2012). Addressing the Terawatt Challenge: Scalability in the Supply of Chemical Elements for Renewable Energy. *RSC Advances, 2(21),* Pp. 7933. DOI:10.1039/c2ra20839c

36 Vesborg, P. C. K., Seger, B., & Chorkendorff, I. (2015). Recent Development in Hydrogen Evolution Reaction Catalysts and Their Practical Implementation. *The Journal of Physical Chemistry Letters, 6(6),* Pp. 951–957. DOI:10.1021/acs.jpclett.5b00306

37 Wan, C. & Leonard, M. (2015). Iron-Doped Molybdenum Carbide Catalyst with High Activity and Stability for the Hydrogen Evolution Reaction. *Chemistry of Materials, 27(12),* Pp. 4281–4288. DOI: 10.1021/acs.chemmater.5b0062 38

38 Wan, C., Regmi, Y. N., & Leonard, B. M. (2014). Multiple Phases of Molybdenum Carbide as Electrocatalysts for the Hydrogen Evolution Reaction. *Angewandte Chemie, 126(25),* Pp. 6525–6528. DOI:10.1002/ange.201402998

39 Wang, Y., Qiu, W., Song, E., Gu, F., Zheng, Z., Zhao, X., Zhao, Y., Liu, J., & Zhang, W. (2017). Adsorption-Energy-Based Activity Descriptors for Electrocatalysts in Energy Storage Applications. *National Science Review, 5(3),* Pp. 327–341. DOI:10.1093/nsr/nwx119

40 Xie, J., Zhang, J., Li, S., Grote, F., Zhang, X., Zhang, H., Wang, R., Lei, Y., Pan, B., & Xie, Y.(2013). Controllable Disorder Engineering in Oxygen-Incorporated MoS2 Ultrathin Nanosheets for Efficient Hydrogen Evolution. *Journal of the American Chemical Society, 135(47).* Pp. 17881–17888. DOI: 10.1021/ja408329q

41 Xie, Y. P., Liu, G., Yin, L., & Cheng, H. M. (2012). Crystal Facet-Dependent Photocatalytic Oxidation and Reduction Reactivity of Monoclinic WO3 for Solar Energy Conversion. *Journal of Materials Chemistry, 22(14).* Pp. 6746-6751. DOI: 10.1039/C2JM16178H

42 Xu, C., Peng, S., Tan, C., Ang, H., Tan, H., Zhang, H., & Yan, Q. (2014). Ultrathin S-doped MoSe2 Nanosheets for Efficient Hydrogen Evolution. *Journals of Materials Chemistry A, 2(16).* Pp. 5597-5601. DOI: 10.1039/c4ta00458b

43 Yang, L., Wu, X., Zhu, X., He, C., Meng, M., Gan, Z., & Chu, P. K. (2015). Amorphous Nickel/Cobalt Tungsten Sulfide Electrocatalysts for High-Efficiency Hydrogen Evolution Reaction. *Applied Surface Science*, Pp. 341, 149–156. DOI:10.1016/j.apsusc.2015.03.018

44 Yu, L., Deng, D., & Bao, X. (2020). Chain Mail for Catalysts. *Angewandte Chemie, 132(36).* Pp. 15406-15409. DOI: 10.1002/ange.202007604

45 Yue, M., Lambert, H., Pahon, E., Roche, R., Jemei, S., & Hissel, D. (2021). Hydrogen Energy Systems: A Critical Review of Technologies, Applications, Trends and Challenges. *Renewable and Sustainable Energy Reviews, 146,* Pp. 111180. DOI:10.1016/j.rser.2021.111180

46 Zeng, M., & Li, Y. (2015). Recent Advances in Heterogeneous Electrocatalysts for the Hydrogen Evolution Reaction. *Journal of Materials Chemistry A, 3(29),* Pp. 14942–14962. DOI:10.1039/c5ta02974k

47 Zhang J, Wang T, Liu P, Liu S, Dong R, Zhuang X, Chen M, & Feng X (2016). Engineering Water Dissociation Sites in MoS2 Nanosheets for Accelerated Electrocatalytic Hydrogen Production. *Energy Environment Science, 9(9).* Pp.2789. DOI: 10.1039/C6EE01786J

48 Zhang, K., Li, Y., Deng, S., Shen, S., Zhang, Y., Pan, G., Xiong, Q., Liu, Q., Xia, X., Wang, W., & Tu, J. (2019). Molybdenum Selenide Electrocatalysts for Electrochemical Hydrogen Evolution Reaction. *ChemElectroChem, 6.* Pp. 3530 – 3548. DOI: 10.1002/celc.201900448

49 Zhou, X., Jiang, J., Ding, T., Zhang, J., Pan, B., Zuo, J. & Yang, Q. (2014). Fast Colloidal Synthesis of Scalable Mo-Rich Hierarchical Ultrathin MoSe2−*x* Nanosheets for High-Performance Hydrogen Evolution. *Nanoscale, 6(19),* Pp. 11046–11051. DOI: 10.1039/c4nr02716g

50 Zhuang, Z., Huang, J., Li, Y., Zhou, L., & Mai, L. (2019). The Holy Grail in Platinum-Free Electrocatalytic Hydrogen Evolution: Molybdenum-Based Catalysts and Recent Advances. *ChemElectroChem, 6.* Pp. 3570 – 3589. DOI: 10.1002/celc.201900143